

The Lack of Synapsin Alters Presynaptic Plasticity at Hippocampal Mossy Fibers in Male Mice

 Felicitas Bruentgens,^{1,2}  Laura Moreno Velasquez,^{1,2*} Alexander Stumpf,^{1,2*}  Daniel Parthier,^{1,2,3}  Jörg Breustedt,^{1,2}  Fabio Benfenati,^{4,5}  Dragomir Milovanovic,^{1,6,7}  Dietmar Schmitz,^{1,2,3,6,7,8} and  Marta Orlando^{1,2}

¹Charité – Universitätsmedizin Berlin, corporate member of Freie Universität Berlin and Humboldt-Universität zu Berlin, Berlin 10117, Germany, ²NeuroCure Cluster of Excellence, Charité – Universitätsmedizin Berlin, corporate member of Freie Universität Berlin and Humboldt-Universität zu Berlin, Berlin 10117, Germany, ³Max Delbrück Center for Molecular Medicine in the Helmholtz Association, Berlin 13125, Germany, ⁴Center for Synaptic Neuroscience and Technology, Istituto Italiano di Tecnologia, Genoa 16163, Italy, ⁵IRCCS Ospedale Policlinico San Martino, Genoa 16132, Italy, ⁶German Center for Neurodegenerative Diseases (DZNE) Berlin, Berlin 10117, Germany, ⁷Einstein Center for Neurosciences, Charité – Universitätsmedizin Berlin, corporate member of Freie Universität Berlin and Humboldt-Universität zu Berlin, Berlin 10117, Germany, and ⁸Bernstein Center for Computational Neuroscience, Humboldt-Universität zu Berlin, Berlin 10115, Germany

Abstract

Synapsins are highly abundant presynaptic proteins that play a crucial role in neurotransmission and plasticity via the clustering of synaptic vesicles. The synapsin III isoform is usually downregulated after development, but in hippocampal mossy fiber boutons, it persists in adulthood. Mossy fiber boutons express presynaptic forms of short- and long-term plasticity, which are thought to underlie different forms of learning. Previous research on synapsins at this synapse focused on synapsin isoforms I and II. Thus, a complete picture regarding the role of synapsins in mossy fiber plasticity is still missing. Here, we investigated presynaptic plasticity at hippocampal mossy fiber boutons by combining electrophysiological field recordings and transmission electron microscopy in a mouse model lacking all synapsin isoforms. We found decreased short-term plasticity, i.e., decreased facilitation and post-tetanic potentiation, but increased long-term potentiation in male synapsin triple knock-out (KO) mice. At the ultrastructural level, we observed more dispersed vesicles and a higher density of active zones in mossy fiber boutons from KO animals. Our results indicate that all synapsin isoforms are required for fine regulation of short- and long-term presynaptic plasticity at the mossy fiber synapse.

Key words: hippocampal mossy fibers; presynaptic plasticity; presynaptic potentiation; synapsin; synaptic transmission; synaptic vesicles

Significance Statement

Synapsins cluster vesicles at presynaptic terminals and shape presynaptic plasticity at giant hippocampal mossy fiber boutons. Deletion of all synapsin isoforms results in decreased short- but increased long-term plasticity.

Introduction

Neurotransmission is a fundamental process that enables us to sense the world around us, to react to it, and to think, learn and remember. This process requires high temporal and spatial fidelity, and the energy-expensive and complex regulation of synaptic vesicle trafficking is a prerequisite. A crucial aspect is the spatial arrangement of

Received Aug. 29, 2023; revised May 17, 2024; accepted May 20, 2024.

The authors declare no competing financial interests.

Author contributions: D.S. and M.O. designed research; Felicitas Bruentgens, L.M.V., A.S., and M.O. performed research; Fabio Benfenati and D.M. contributed unpublished reagents/analytic tools; Felicitas Bruentgens, L.M.V., A.S., D.P., J.B. and M.O. analyzed data; Felicitas Bruentgens and M.O. wrote the paper.

This study was supported by the Deutsche Forschungsgemeinschaft (DFG, German Research Foundation), project 184695641, SFB 958 (to D.S.); project 327654276, SFB 1315 (to D.S.); project 415914819, FOR 3004 (to D.S.); project 431572356 (to D.S.), under Germany's Excellence Strategy EXC-2049-390688087 (NeuroCure; to D.S. and M.O.); and project 503954250 (to M.O.). It was also supported by the European Research Council (ERC) under the European Union's Horizon 2020 research and innovation program (BrainPlay Grant Agreement No. 810580; to D.S.) and by the Federal Ministry of Education and Research (BMBF, SmartAge, Project 01GQ1420B; to D.S.). D.M. is

Continued on next page.

neurotransmitter-filled vesicles inside the synapse, regulated by the protein family of synapsins (Atias et al., 2019; Sansevrino et al., 2023).

Synapsins are highly abundant phosphoproteins associated with the surface of synaptic vesicles (De Camilli et al., 1990; Cesca et al., 2010), encoded by three mammalian genes (*SYN1*, *SYN2*, *SYN3*; Südhof et al., 1989; Kao et al., 1998). The lack of synapsin I (SynI) and II (SynII) causes vesicle dispersion and shrinks the distal vesicle cluster, the reserve pool (Li et al., 1995; Pieribone et al., 1995; Rosahl et al., 1995). Thus, a major function of synapsins is to control mobilization from the reserve pool, in a phosphorylation-dependent manner (Sihra et al., 1989; Hosaka et al., 1999; Chi et al., 2001). How synapsins preserve this pool is still under debate. Likely mechanisms are: (1) synapsins cross-link the vesicles, acting as tethers (Hirokawa et al., 1989); (2) synapsins form a liquid phase, capturing vesicles in it (Milovanovic et al., 2018; Pechstein et al., 2020); or (3) a mixture of both, since these mechanisms are not mutually exclusive (Zhang and Augustine, 2021; Song and Augustine, 2023; Longfield et al., 2024).

While SynI and SynII are expressed in mature synapses (De Camilli et al., 1983; Browning et al., 1987), synapsin III (SynIII) is primarily expressed during development: after 1 week postnatal its levels decrease drastically (Ferreira et al., 2000) and remain low in adults (Kao et al., 1998). However, in brain regions featuring postnatal neurogenesis, SynIII is still expressed in the adult tissue (Pieribone et al., 2002). This includes the dentate gyrus and hippocampal mossy fibers.

Hippocampal mossy fibers are involved in learning, memory, and spatial navigation (Lassalle et al., 2000; Rolls, 2018). They connect granule cells and CA3 pyramidal cells via mossy fiber boutons, highly plastic synapses (Nicoll and Schmitz, 2005). Activity-dependent changes in neurotransmission can be studied very well in these boutons, because they can react to a wide range of frequencies (Salin et al., 1996) and express presynaptic short- and long-term potentiation (STP, LTP; Zalutsky and Nicoll, 1990; Nicoll and Schmitz, 2005). Recently, a mechanism for short-term memory has been proposed: the formation of a “pool engram”—an increased readily releasable pool (RRP)—which could depend on the vesicle mobilization via synapsins (Vandael et al., 2020). Unlike STP, mossy fiber LTP is still more enigmatic: it is known to be protein kinase A (PKA)-dependent (Weisskopf et al., 1994), but the precise downstream targets and potential parallel mechanisms are not yet clarified (Monday et al., 2018, 2022; Shahoha et al., 2022).

Synapsin-dependent mossy fiber physiology has been investigated in SynI/SynII double knock-out (SynDKO) animals (Spillane et al., 1995; Owe et al., 2009): field recordings revealed impaired frequency facilitation in physiologically relevant ranges (Owe et al., 2009), while LTP was unchanged (Spillane et al., 1995). However, enrichment of SynIII close to the active zone at mossy fiber boutons (Owe et al., 2009) raised the question if the complete knock-out (KO) of synapsins would have further effects on mossy fiber transmission and plasticity.

Here, we examined a glutamatergic synapse that retains SynIII expression in adulthood and asked how neurotransmission and synaptic morphology are changed upon the complete loss of synapsins. We investigated this question in acute slices of SynI/SynII/SynIII triple KO (SynTKO) male mice using a combined approach of transmission electron microscopy (TEM) and electrophysiological field recordings. We observed fewer vesicles in the reserve pool and increased active zone density. Field recordings provided evidence that synapsins are crucial for both STP and LTP in mossy fibers: facilitation and post-tetanic potentiation (PTP) were impaired, while LTP was enhanced.

Materials and Methods

Reporting guidelines

This study was reported in accordance with the Sex and Gender Equity in Research (SAGER) guidelines (Heidari et al., 2016) and Animal Research: Reporting of In Vivo Experiments (ARRIVE) guidelines 2.0 (Percie du Sert et al., 2020). The checklist for the SAGER guideline is provided in Table 1, the checklist for the essential 10 of the ARRIVE guideline is provided in Table 2, and the checklist for the recommended set of the ARRIVE guideline is provided in Table 3.

Ethics statement

All animal experiments were carried out according to the guidelines stated in Directive 2010/63/EU of the European Parliament on the protection of animals used for scientific

supported by the startup funds from DZNE, the grants from the German Research Foundation (317475864; SFB 1286/B10 and MI 2104), and the Human Frontiers Science Organization (RGEC32/2023). The funders had no role in study design, data collection and analysis, decision to publish, or preparation of the manuscript. We thank Susanne Rieckmann for her excellent technical assistance. We thank Anke Schönherr and Caterina Michetti for organizational matters with SynTKO animals as well as Christian Hoffmann and Franziska Trnka for their assistance in obtaining the necessary animal permits for the SynTKO line. We thank the Electron Microscopy Laboratory of the Institute of Integrative Neuroanatomy and the Core Facility for Electron Microscopy of the Charité for granting us access to their instruments. We thank René Bernard for his valuable input on Open Science. Finally, we thank Antje Fortströer for the careful revision of our manuscript.

*L.M.V. and A.S. contributed equally to this work.

Correspondence should be addressed to Marta Orlando at marta.orlando@charite.de or Dietmar Schmitz at dietmar.schmitz@charite.de.

Copyright © 2024 Bruentgens et al. This is an open-access article distributed under the terms of the [Creative Commons Attribution 4.0 International license](https://creativecommons.org/licenses/by/4.0/), which permits unrestricted use, distribution and reproduction in any medium provided that the original work is properly attributed.

Table 1. SAGER guidelines checklist, other studies (applied sciences, cell biology, etc.)

Section/topic	Item number	Checklist item	Reported on page number
General	1	The terms sex/gender used appropriately	Does not apply
Title	2a	Title specifies the sex of animals or any cells, tissues, and other material derived from these	1
	2b	In applied sciences (technology, engineering, etc.), the title indicates if the study model was based on one sex/gender or the application was considered for the use of one specific sex/gender	Does not apply
Abstract	3a	Abstract specifies sex of animals or any cells, tissues, and other material derived from these	4
	3b	In applied sciences (technology, engineering, etc.), the abstract indicates if the study model was based on one sex/gender or the application was considered for the use of one specific sex/gender	Does not apply
Introduction	4a	If relevant, previous studies that show presence or lack of sex or gender differences or similarities are cited	Does not apply
	4b	Mention of whether sex/gender might be an important variant and if differences might be expected	Not performed
Materials and Methods	5a	In cell biological, molecular biological, or biochemical experiments, the origin and sex chromosome constitutions of cells or tissue cultures are stated. If unknown, the reasons are stated	Does not apply
	5b	For studies testing devices or technology, explanation of whether the product will be applied or used by all genders and if it has been tested with a user's gender in mind	Does not apply
	5c	If relevant, description of how sex/gender was considered in the design	Does not apply
	5d	For in vivo and in vitro studies using primary cultures of cells, or cell lines from humans or animals, or ex vivo studies with tissues from humans or animals, the sex of the subjects or source donors is stated (except for immortalized cell lines, which are highly transformed)	7
Results	6	For studies using animal models, present a sex breakdown of the animals ^a	Does not apply
Discussion	7	If relevant, potential implications of sex/gender on the study results and analyses, including the extent to which the findings can be generalized to all sexes/genders in a population	28

Adapted from Heidari et al. (2016).

^aThese points extend beyond the original SAGER table.

purposes and were approved by the animal welfare committee of Charité – Universitätsmedizin Berlin and the Landesamt für Gesundheit und Soziales Berlin (permit T 0100/03 and permit G 0146/20).

Study design

In this study, only male mice were used for experiments to exclude possible indirect estrogen effects on mossy fiber plasticity (Harte-Hargrove et al., 2013). In electrophysiological recordings, C57BL/6J control mice [research resource identifier (RRID):IMSR_JAX:000664] were compared with SynTKO mice (RRID:MMRRC_041434-JAX) in two age groups: one younger group (4–6 weeks of age), which is referred to as presymptomatic, and one older group (17–19 weeks of age), which is referred to as symptomatic. These terms describe the phenotype before and after the onset of epileptic seizures in SynTKO animals, respectively (Farisello et al., 2013). SynTKO mice were purchased from the Jackson Laboratory (RRID:SCR_004633) and were based on the work of Gitler and coworkers (Gitler et al., 2004). The presymptomatic SynTKO data were obtained from two different cohorts. We received the first cohort from Prof. Dr. Fabio Benfenati (Istituto Italiano di Tecnologia). The second cohort from Dr. Dragomir Milovanovic (DZNE) was housed and bred in the Charité animal facility (Forschungseinrichtungen für Experimentelle Medizin). Symptomatic SynTKO animals and all control animals were also bred and born in the Charité animal facility. For each experiment, we were aiming for at least three biological replicates (animals) per group. Depending on experimental success (how many recordings needed to be excluded, technical failures), we added more animals per group.

Field recordings. Data from both presymptomatic SynTKO cohorts were pooled, because they were not significantly different (Table 4). Field recording experiments in all four groups [wild-type (WT), SynTKO, presymptomatic, symptomatic] were repeated with at least three mice from more than one litter (Table 5). Variable *s* represents the number of recorded slices, while *a* reports the number of animals. We were not blinded toward the genotype, because the phenotype was too strong.

Recordings were excluded when they had a baseline field excitatory postsynaptic potential (fEPSP) smaller than two times noise (Table 6). Noise was ~25 μV , so the baseline fEPSP amplitude needed to be at least 50 μV to be included. Furthermore,

Table 2. The ARRIVE guidelines 2.0 checklist: the essential 10

Item	Item number	Recommendation	Reported in section
Study design	1	a. For each experiment, provide brief details of study design including: the groups being compared, including control groups. If no control group has been used, the rationale should be stated	Materials and Methods, Study design and Results
		b. The experimental unit (e.g., a single animal, litter, or cage of animals)	Materials and Methods, Study design and Table 5
Sample size	2	a. Specify the exact number of experimental units allocated to each group and the total number in each experiment. Also indicate the total number of animals used	Materials and Methods, Study design and Table 5
		b. Explain how the sample size was decided. Provide details of any a priori sample size calculation, if done	Materials and Methods, Study design
Inclusion and exclusion criteria	3	a. Describe any criteria used for including and excluding animals (or experimental units) during the experiment and data points during the analysis. Specify if these criteria were established a priori. If no criteria were set, state this explicitly	Materials and Methods, Field recordings
		b. For each experimental group, report any animals, experimental units, or data points not included in the analysis and explain why. If there were no exclusions, state so	Materials and Methods, Tables 5 and 6
		c. For each analysis, report the exact value of n in each experimental group.	Materials and Methods, Study design and Table 5
Randomization	4	a. State whether randomization was used to allocate experimental units to control and treatment groups. If done, provide the method used to generate the randomization sequence	Materials and Methods, Study design
		b. Describe the strategy used to minimize potential confounders such as the order of treatments and measurements or animal/cage location. If confounders were not controlled, state this explicitly	Materials and Methods, Study design
Blinding	5	Describe who was aware of the group allocation at the different stages of the experiment (during the allocation, the conduct of the experiment, the outcome assessment, and the data analysis)	Materials and Methods, Study design
Outcome measures	6	a. Clearly define all outcome measures assessed (e.g., cell death, molecular markers, or behavioral changes)	Results; Materials and Methods, TEM and Table 5
		b. For hypothesis-testing studies, specify the primary outcome measure, i.e., the outcome measure that was used to determine the sample size	Does not apply
Statistical methods	7	a. Provide details of the statistical methods used for each analysis, including the software used	Materials and Methods, Statistics
		b. Describe any methods used to assess whether the data met the assumptions of the statistical approach and what was done if the assumptions were not met	Materials and Methods, Statistics
Experimental animals	8	a. Provide species-appropriate details of the animals used, including species, strain and substrain, sex, age or developmental stage, and, if relevant, weight	Materials and Methods, Study design and key resources table
		b. Provide further relevant information on the provenance of animals, health/immune status, genetic modification status, genotype, and any previous procedures	Materials and Methods, Study design; Results; Discussion
Experimental procedures	9	a. For each experimental group, including controls, describe the procedures in enough detail to allow others to replicate them, including: what was done, how it was done, and what was used	Materials and Methods
		b. When and how often	Materials and Methods, TEM, Table 5
		c. Where (including detail of any acclimatization periods)	Materials and Methods, Acute slice preparation, Field recordings, and TEM
		d. Why (provide rationale for procedures)	Introduction; Results; Discussion; Materials and Methods (<i>Table continues.</i>)

Table 2. Continued

Item	Item number	Recommendation	Reported in section
Results	10	a. For each experiment conducted, including independent replications, report the summary/descriptive statistics for each experimental group, with a measure of variability where applicable (e.g., mean and SD or median and range)	Results, text and figure legends
		b. If applicable, the effect size with a confidence interval	Does not apply

Adapted from Percie du Sert et al. (2020).

Table 3. The ARRIVE guidelines 2.0: the recommended set

Item	Item number	Recommendation	Reported in section
Abstract	11	Provide an accurate summary of the research objectives, animal species, strain and sex, key methods, principal findings, and study conclusions	Abstract
Background	12	a. Include sufficient scientific background to understand the rationale and context for the study, and explain the experimental approach	Introduction; Results; Discussion
		b. Explain how the animal species and model used address the scientific objectives and, where appropriate, the relevance to human biology	Introduction; Results; Discussion
Objectives	13	Clearly describe the research question, research objectives, and, where appropriate, specific hypotheses being tested	Abstract; Introduction; Results; Discussion
Ethical statement	14	Provide the name of the ethical review committee or equivalent that has approved the use of animals in this study and any relevant license or protocol numbers (if applicable). If ethical approval was not sought or granted, provide a justification	Materials and Methods, Ethics statement
Housing and husbandry	15	Provide details of housing and husbandry conditions, including any environmental enrichment	Materials and Methods, Acute slice preparation
Animal care and monitoring	16	a. Describe any interventions or steps taken in the experimental protocols to reduce pain, suffering, and distress	Materials and Methods, Acute slice preparation
		b. Report any expected or unexpected adverse events	Does not apply
		c. Describe the humane endpoints established for the study, the signs that were monitored, and the frequency of monitoring. If the study did not have humane endpoints, state this	Not performed
Interpretation/scientific implications	17	a. Interpret the results, taking into account the study objectives and hypotheses, current theory, and other relevant studies in the literature	Discussion
		b. Comment on the study limitations including potential sources of bias, limitations of the animal model, and imprecision associated with the results	Discussion
Generalizability/translation	18	Comment on whether, and how, the findings of this study are likely to generalize to other species or experimental conditions, including any relevance to human biology (where appropriate)	Discussion
Protocol registration	19	Provide a statement indicating whether a protocol (including the research question, key design features, and analysis plan) was prepared before the study and if and where this protocol was registered	Not performed
Data access	20	Provide a statement describing if and where study data are available	Data Availability
Declaration of interests	21	a. Declare any potential conflicts of interest, including financial and non-financial. If none exist, this should be stated	Conflict of interest statement
		b. List all funding sources (including grant identifier) and the role of the funder(s) in the design, analysis, and reporting of the study	Acknowledgments

Adapted from Percie du Sert et al. (2020).

to include only mossy fiber-specific recordings, we applied 1 μ M (2*S*,1'*R*,2'*R*,3'*R*)-2-(2,3-dicarboxycyclopropyl)glycine (DCG-IV; 0975, Tocris Bioscience) at the end of each experiment (Kamiya et al., 1996). If the suppression was 75% or more, the recording was included (Table 6). We were not able to measure input–output curves for all animals. For those

Table 4. Statistical comparison for experimental values between two cohorts of presymptomatic SynTKO animals

Experiment	Measure	Presynaptic SynTKO animals from Italy	Presynaptic SynTKO animals from Berlin
Input–output	Slope of simple linear regression	1.341	0.833
	Ranges of 95% confidence band	0.5494–2.134	0.09287–1.573
1 Hz facilitation	<i>p</i> value slopes (ANCOVA)		0.69
	Median	4.440	5.955
	Interquartile range	3.760–6.260	3.753–11.41
PPR	<i>p</i> value (Mann–Whitney U test)		0.3473
	Median	3.557	4.545
	Interquartile ranges	2.299–4.260	2.568–6.035
PTP (norm. fEPSP)	<i>p</i> value (Mann–Whitney U test)		0.0899
	Median	3.469	4.116
	Interquartile ranges	2.118–4.589	3.374–7.144
LTP after 30 min (norm. fEPSP)	<i>p</i> value (Mann–Whitney U test)		0.1151
	Median	245.2	228.8
	Interquartile ranges	198.3–302.9	182.5–384.4
	<i>p</i> value (Mann–Whitney U test)		0.8793

Table 5. Overview of slice and animal numbers for different experimental groups for field recordings

<i>s</i> = number of slices <i>a</i> = number of animals	C57BL/6J (4–6 weeks)	Synapsin TKO (4–6 weeks)		C57BL/6J (17–19 weeks)	Synapsin TKO (18–19 weeks)
		From Italy (4–5 weeks)	From Berlin (4–6 weeks)		
Recorded	<i>s</i> = 67 <i>a</i> = 12	<i>s</i> = 39 <i>a</i> = 9	<i>s</i> = 18 <i>a</i> = 7	<i>s</i> = 29 <i>a</i> = 5	<i>s</i> = 24 <i>a</i> = 5
Included	<i>s</i> = 31 <i>a</i> = 12	<i>s</i> = 24 <i>a</i> = 9	<i>s</i> = 14 <i>a</i> = 4	<i>s</i> = 17 <i>a</i> = 4	<i>s</i> = 19 <i>a</i> = 5
Input–output ratio	<i>s</i> = 31 <i>a</i> = 12	<i>s</i> = 23 <i>a</i> = 9	<i>s</i> = 14 <i>a</i> = 4	<i>s</i> = 17 <i>a</i> = 4	<i>s</i> = 18 <i>a</i> = 5
PPR	<i>s</i> = 31 <i>a</i> = 12	<i>s</i> = 20 <i>a</i> = 8	<i>s</i> = 14 <i>a</i> = 4	<i>s</i> = 17 <i>a</i> = 4	<i>s</i> = 19 <i>a</i> = 5
1 Hz facilitation	<i>s</i> = 31 <i>a</i> = 12	<i>s</i> = 15 <i>a</i> = 5	<i>s</i> = 12 <i>a</i> = 4	<i>s</i> = 17 <i>a</i> = 4	<i>s</i> = 19 <i>a</i> = 5
25 Hz stimulation	<i>s</i> = 11 <i>a</i> = 5	<i>s</i> = 4 <i>a</i> = 3	<i>s</i> = 8 <i>a</i> = 3		
PTP + LTP	<i>s</i> = 15 <i>a</i> = 6	<i>s</i> = 13 <i>a</i> = 6	<i>s</i> = 10 <i>a</i> = 3		

Note: all numbers reported for individual experiments are only from the included subset of recordings.

Table 6. Exclusion reasons for field recordings

Excluded recordings	C57BL/6J (4–6 weeks)	Synapsin TKO (4–6 weeks)	C57BL/6J (17–19 weeks)	Synapsin TKO (18–19 weeks)
Baseline fEPSP <50 μ V	4	2	2	2
DCG-IV effect <75%	27	14	11	4
Other reasons	6	2	0	1
Total number	36	19	12	5

Note that several reasons can apply to the same recording.

cases where it was not recorded with different input strengths, we plotted only one value based on the averaged baseline values for presynaptic fiber volley (PFV) and fEPSP, respectively. If the PFV could not be measured unambiguously, this measurement was excluded from the input–output graph. If the 1 or 25 Hz induction failed, the respective measurements were excluded from analysis, but all other parameters from the same experiment were included. The same was true for some recordings, in which no 25 Hz stimulation and thus no PTP and LTP recordings were conducted. Due to the pooled data from the two presymptomatic SynTKO cohorts, there is an imbalance between numbers from WT and numbers from

SynTKO animals in high-frequency recordings. If possible, two mice with different genetic backgrounds were recorded on the same day to minimize variability due to experimental day.

Transmission electron microscopy. For ultrastructural investigation of mossy fiber boutons, we analyzed mossy fiber boutons from three WT and three SynTKO male mice aged 4–6 weeks. Mice from the two presymptomatic SynTKO cohorts were pooled. We imaged serial sections from 18 WT and 16 SynTKO mossy fiber boutons, respectively. We measured bouton complexity, vesicle number, and mean nearest neighbor distance (MNND) between vesicles in 2D images. Measures of active zone density, active zone area, and docked synaptic vesicle density were obtained by manually annotating partial 3D reconstructions of mossy fiber boutons (total volume of presynaptic boutons analyzed, $48.2 \mu\text{m}^3$; average volume of each fraction of presynaptic bouton, $0.72 \pm 0.28 \mu\text{m}^3$; data not shown). Slices from each animal were either treated with forskolin (FSK) or allocated as the control. Allocation of slices to the treatment or control group was block-randomized. Replicates of 17 (WT), 16 (WT + FSK), 16 (SynTKO), and 18 (SynTKO + FSK) mossy fiber boutons were analyzed. Number n represents the number of partial presynaptic bouton reconstructions. The experimenter was blinded to the treatment of slices from fixation of the slices until the end of analysis. Due to the strong reduction in vesicle density of SynTKO synapses, blinding during analysis was only possible between treatment groups, but not between genotypes.

Acute slice preparation

Animals were kept in a 12/12 h light/dark cycle, and water and food were provided *ad libitum*. Cages offered shelter in the form of a house and tubes. Cages of SynTKO animals were kept in remote shelves to minimize exposure to light and possible noises. The first cohort of presymptomatic SynTKO animals was imported from Italy and allowed to sit in the Charité animal facility for several days before the experiments started. After the transfer from the animal facility to the preparation room, all animals were allowed to acclimate to the new surroundings for at least half an hour. Acute brain slices were prepared as follows: mice were anesthetized under the hood with isoflurane and quickly killed with sharp scissors. The brain was taken out and placed in oxygenated ice-cold sucrose–artificial cerebrospinal fluid (S-ACSF) for 3 min to allow equilibration. S-ACSF contained the following (in mM): 50 NaCl, 25 NaHCO₃, 10 glucose, 150 sucrose, 2.5 KCl, 1 NaH₂PO₄, 0.5 CaCl₂, 7 MgCl₂. All solutions were saturated with 95% O₂ (v/v)/5% CO₂ (v/v) and had a pH of 7.4 and an osmolarity of 340 mOsm. Hemispheres were separated, and 300 μm /150 μm (field recordings/electron microscopy) thick sagittal sections were cut from both hemispheres with a vibratome [VT1200 S, Leica Biosystems (RRID: SCR_018453)]. Slices were stored in a submerged chamber in oxygenated S-ACSF at 34°C for half an hour before they were moved to another submerged chamber with ACSF at room temperature. There, slices were kept until the start of experiments. ACSF had an osmolarity of 300 mOsm and a pH of 7.4 and contained (in mM): 119 NaCl, 26 NaHCO₃, 10 glucose, 2.5 KCl, 1 NaH₂PO₄, 2.5 CaCl₂, 1.3 MgCl₂. All chemicals were purchased from Sigma-Aldrich.

Field recordings

Slices were kept in a submerged chamber with ACSF at least 30 min and up to 8 h before the start of recordings. Slices were placed in a recording chamber under a microscope and were continuously superfused with oxygenated ACSF at room temperature at a rate of ~ 2.5 ml/min. The recording electrode was fixed in a headstage of the amplification system [Axon Instruments, MultiClamp 700A/700B (RRID:SCR_018455)]. Stimulation and recording electrode units were placed on micromanipulators (Mini 23/25, Luigs & Neumann) for a precise movement control via a control system (SM-5/-7/-10, Luigs & Neumann).

The stimulation and recording electrodes were prepared from silver wires (AG-8W and E-205, Science Products). Glass pipettes were made from borosilicate capillaries (GB150EFT-10, Science Products or 1403005, Hilgenberg) with a pipette puller (PC-10, Narishige or DMZ-Universal Puller, Zeitz-Instrumente) and were broken at the tip with a micro forge (MF-830, Narishige) to receive low-resistance pipettes. Electrodes were placed in the hilus of the dentate gyrus near the granule cell layer (stimulation) and within the *stratum lucidum* of the area CA3 of the hippocampus (recording), respectively.

Stimulations were executed with a stimulation box [ISO-Flex, AMPI (RRID:SCR_018945)], and stimulation patterns were controlled with a Master-8 generator [AMPI (RRID:SCR_018889)]. Igor Pro [version 6, WaveMetrics (RRID:SCR_000325)] was used for signal acquisition. The Axon MultiClamp amplifier [700A/700B, Molecular Devices (RRID:SCR_018455)] was used in the current clamp mode $I=0$, with filtering of 2 kHz. Signals were digitized (Axon Digidata 1550B, Molecular Devices/BNC-2090; National Instruments Germany) at a rate of 20 kHz. Mossy fiber signals were searched by placing the stimulation and recording electrodes at different locations in the hilus and stratum lucidum, respectively. Once a mossy fiber input was obtained, the recording was started, and the mossy fibers were stimulated at 0.05 Hz.

The standard stimulation frequency was 0.05 Hz throughout the experiment, unless otherwise stated. The recorded sweep length was 0.5 s except for the high-frequency stimulation at 25 Hz where 5.5 s were recorded. First, input–output relations were recorded by applying different input currents via the stimulation box. The strength of the input current was adjusted to yield a specific PFV size: 0.05 mV, 0.1 mV, 0.2 mV, 0.3 mV and maximum (maximal stimulation strength of 10 mA). Each input strength was recorded for three sweeps. Afterward, a medium stimulation strength was chosen, and a baseline was recorded for at least 10 sweeps. Then, the stimulation frequency was increased to 1 Hz for 20 sweeps for recording of frequency facilitation. Afterwards, when fEPSP amplitudes declined to baseline level again, a paired-pulse

with an interstimulus interval of 50 ms was applied for three sweeps. Then, a baseline was recorded for 10 min (30 sweeps, except for once when only 20 sweeps were recorded) before a high-frequency train of stimuli was given: four times 125 pulses at 25 Hz every 20 s with a recorded sweep length of 5.5 s. PTP and subsequently LTP were measured for at least 30 min after the tetanus. Mossy fiber purity of signals was verified at the end of each recording with the application of 1 μ M DCG-IV (0975, Tocris Bioscience). All recordings with a suppression of at least 75% of the signal were used for analysis.

Field recording analysis

Field recordings were analyzed with Igor Pro [versions 6 and 8, WaveMetrics (RRID:SCR_000325)] and the installed plugin NeuroMatic (RRID:SCR_004186) as well as Microsoft Excel (RRID:SCR_016137). Igor Pro is commercially available at <https://www.wavemetrics.com/products/igorpro>, and Microsoft Excel is commercially available at <https://www.microsoft.com/de-de/microsoft-365/excel>. PFVs were measured from peak to peak. fEPSP amplitudes were baseline-corrected and measured ± 2 ms around the peak. For input–output curves, the mean value of the three sweeps at the same stimulation strength was taken, except for the cases in which no input–output curve was recorded: here, we took the average size of PFV and fEPSP amplitudes from the initial baseline. fEPSP amplitudes during 1 Hz facilitation were normalized to the initial baseline (10 sweeps, 3 min). The paired-pulse ratio (PPR) was calculated as the ratio between the second to the first fEPSP amplitude. The stated PPR refers to the first of three paired stimulations. For analysis of the high-frequency trains, we normalized the fEPSP amplitudes to the baseline before (30 sweeps, 10 min). We also evaluated the PFV size for a subset of fEPSPs of the 25 Hz trains. We measured the PFV for stimuli 10–15 and averaged those six values for the first and fourth stimulation train, respectively (Fig. 2f). Also, we calculated the ratio of those averaged values between fourth and first stimulation train, to compare the relative loss of PFV size (Fig. 2g). Values for PTP and LTP were normalized to the average of the recorded baseline before high-frequency stimulation (30 sweeps, 10 min). Values for LTP were the averaged fEPSP amplitudes from minute 20–30 (30 sweeps) after induction. At the end of the recording, specificity was verified by application of DCG-IV. We averaged the last 15 sweeps of DCG-IV wash-in for quantification. Recordings, in which the suppression was $<75\%$ were not counted as mossy fiber-specific and were not included in the analysis.

Transmission electron microscopy

After preparation, acute slices were allowed to recover in ACSF at room temperature for at least 30 min. Subsequently, we induced chemical LTP in half of the slices by incubating them in 50 μ M forskolin (FSK; AG-CN2-0089-M050, Cayman Chemical), dissolved in DMSO, for 15 min at room temperature in oxygenated ACSF (Orlando et al., 2021). The other half of the slices (controls) were incubated in ACSF containing the same concentration of DMSO as the treatment group. Treatment was allocated following a block randomization design. Subsequently, we moved the slices under a chemical hood where fixation, postfixation, staining, dehydration, and infiltration steps were performed. We fixed proteins by immersing brain slices in a solution containing 1.25% glutaraldehyde (E16216, Science Services) in 66 mM NaCacodylate (E12300, Science Services) buffer for 1 h at room temperature. After extensive washing in 0.1 M NaCacodylate, buffer slices were postfixed in 1% OsO₄ in 0.1 M NaCacodylate buffer for 1 h at room temperature. Slices were then washed and stained en bloc with 1% uranyl acetate (1.08473, Merck Millipore) in dH₂O and dehydrated in solutions with increasing ethanol concentration (70, 80, 96, and 100%). Final dehydration was obtained by incubating slices in propylene oxide [20401, Electron Microscopy Sciences (EMS)]. The infiltration of epoxy resin was obtained by serial incubations in increasing resin/propylene oxide dilutions (1:3; 1:1; 3:1). Samples were finally flat embedded in Epon (E14120-DMP, Science Services) for 48 h at 60°C. The *stratum lucidum* in the CA3 region of the hippocampus was identified in 700nm semithin sections stained with Toluidine blue (Sigma-Aldrich) using a light microscope (Olympus); 70 nm serial sections of these regions of interest were cut with an Ultracut UCT ultramicrotome (Leica Microsystems) equipped with an Ultra 45° diamond knife (DiATOME) and collected on pioloform-coated copper slot grids (EMS2010-Cu, Science Services). If not otherwise stated, all chemicals were purchased from EMS and sold by Science Services.

Electron microscopy imaging of serial sections and 3D reconstructions

A magnification of 7 kx was used to determine the localization of mossy fiber boutons. Subsequently, synapses were imaged at 20 kx (pixel size 2.2 nm) using an EM 900 TEM (Carl Zeiss, RRID:SCR_021364) operated at 80 keV and equipped with a Proscan 2K Slow-Scan CCD-Camera (Carl Zeiss). The *stratum lucidum* of the hippocampal region CA3 was easily distinguishable for the presence of big mossy fiber boutons and for its localization just above the pyramidal cell layer. Mossy fiber boutons were recognized by their large size, their position close to CA3 pyramidal cell bodies, and a large number of presynaptic vesicles (Rollenhagen et al., 2007), including large clear and large dense-core vesicles. Serial images of individual mossy fiber boutons were manually acquired in manually collected serial sections using the ImageSP software (TRS & SysProg) and aligned using the Midas script of the IMOD software (RRID:SCR_003297). The ImageSP software is commercially available at <https://sys-prog.com/en/software-for-science/imagesp/>, and the IMOD software is freely available at <https://bio3d.colorado.edu/imod/>. Synaptic profiles were manually segmented in each image of series belonging to the same mossy fiber bouton. Active zones were identified as the area of the membrane opposite to a post-synaptic density/spine profile and with vesicles attached and accumulated next to the presynaptic membrane.

Active zone analysis

When active zone profiles were visible in at least two sequential serial images, they were traced with the IMOD open line tool and rendered in a 3D model as meshed surfaces. With this criterion we excluded active zones that were only visible in one serial section but included some partially reconstructed active zones that were found at the border of the bouton volume. It is important to note that our partial 3D reconstructions are limited to a fraction of the mossy fiber bouton, measuring, on average, $0.72 \pm 0.28 \mu\text{m}^3$ (data not shown). To account for this limitation, the active zone density values were obtained by normalizing the number of 3D reconstructed active zones to the volume of the presynaptic bouton in the partial reconstruction.

Synaptic vesicle analysis

To analyze synaptic vesicles, we used a machine learning-based algorithm that we had previously developed (Imbrosci et al., 2022). It is freely available at <https://github.com/Imbrosci/synaptic-vesicles-detection>. Briefly, we manually traced the contour of the mossy fiber bouton using Fiji (RRID:SCR_002285), freely available at <https://fiji.sc/>. This approach allowed us to obtain a measure of the bouton area and to create a mask over parts of the image which were not relevant for analysis. Synaptic vesicle analysis was performed automatically in a batch. From all images, the number of vesicles and the MNND were obtained. A tutorial with a demonstration of the tool can be found online at <https://www.youtube.com/watch?v=cvqlcFIdVPw>. A limitation of this approach is that the algorithm detects vesicles attached to the plasma membrane with a lower accuracy compared with how it detects isolated vesicles. To overcome this limitation, we performed a manual analysis of docked vesicles at each 3D reconstructed active zone. The docked vesicle density values were obtained by normalizing the number of docked vesicles to the volume of the presynaptic bouton in the partial reconstruction.

Statistics

For statistical analysis, we used the GraphPad Prism software [GraphPad Prism version 8.4.0 for Windows (RRID:SCR_002798)] and R Project for Statistical Computing (version 4.2.2, RRID:SCR_001905) in RStudio (version 2022.12.0, RRID:SCR_000432). GraphPad Prism is commercially available at <https://www.graphpad.com/>, and R Project for Statistical Computing is freely available at <https://www.r-project.org/>. Distribution of data residuals was visually inspected using a Q–Q plot and/or tested for normality (D'Agostino and Pearson's test) before evaluating them statistically, to understand if the distribution was Gaussian or non-Gaussian. Individual data points are shown as median \pm quartiles, mean values with borders of 95% confidence intervals, or mean \pm SEM. The alpha level for statistical significance was 0.05.

GraphPad Prism. For Figure 1a,e, data points were fitted with a simple linear regression. Slopes of those regressions were tested with a two-tailed ANCOVA and are shown with 95% confidence bands. For Figures 1b,f, 2a,b, and 3a,c, data were tested with a mixed-effects model and a post hoc Sidak's test for multiple comparisons. Factors time, genotype, and the interaction of both were tested. For Figures 1c,d,g,h, 2c,d,g, and 3d, ranks were compared with Mann–Whitney *U* tests. For data in Figure 3b, we used a Kruskal–Wallis test with a post hoc Dunn's correction for multiple comparisons. For Figure 2f we used a Wilcoxon test to compare ranks.

R project for statistical computing in RStudio. One of the central assumptions of many statistical tests is independence of data points, which is not given in a nested experimental design as ours (Galbraith et al., 2010; Krzywinski et al., 2014). Nested structures introduce correlations in the sample, which have to be accounted for, to avoid inflation of false-positive conclusions (Lazic, 2010; Aarts et al., 2014). To account for the multilevel nested structure of the electron microscopy data (Figs. 4c,d, 5d–g), we wrote generalized linear mixed models from the gamma family with a log link. We used the glmer function from the R package: lme4 (RRID:SCR_015654; Bates et al., 2015) to fit the generalized linear mixed models. Nested models were compared with likelihood ratio tests for testing different hypotheses. In case of the data for Figure 5e,g, we performed post hoc tests (marginal contrasts analysis) for multiple comparisons. For obtaining and contrasting the marginal means, we used the R package: emmeans (RRID:SCR_018734). *P* values were adjusted using a false discovery rate correction (Benjamini and Hochberg, 1995). The scripts for the statistical analysis and the corresponding data tables are available on GitHub: https://github.com/FeliBrue/Bruentgens_et_al_2024.

Results

Mossy fibers of SynTKO animals are more excitable

Despite the sparse connectivity (Amaral et al., 1990) and the low baseline activity of granule cells (Jung and McNaughton, 1993), a single mossy fiber bouton is able to trigger the discharge of its postsynaptic partner (Henze et al., 2002; Vyleta et al., 2016). Mossy fiber activity is not only important for pattern separation in the healthy brain (Rolls, 2018) but also for propagation of seizures in the epileptic brain (Nadler, 2003). Since SynTKO animals display high network excitability and develop epileptic seizures at the age of two months (Gitler et al., 2004; Fassio et al., 2011), we tested the excitability in mossy fibers by measuring the input–output relationship. We performed experiments in presymptomatic (4–6 weeks old) and symptomatic (17–19 weeks old) animals, after the onset of epileptic seizures. This

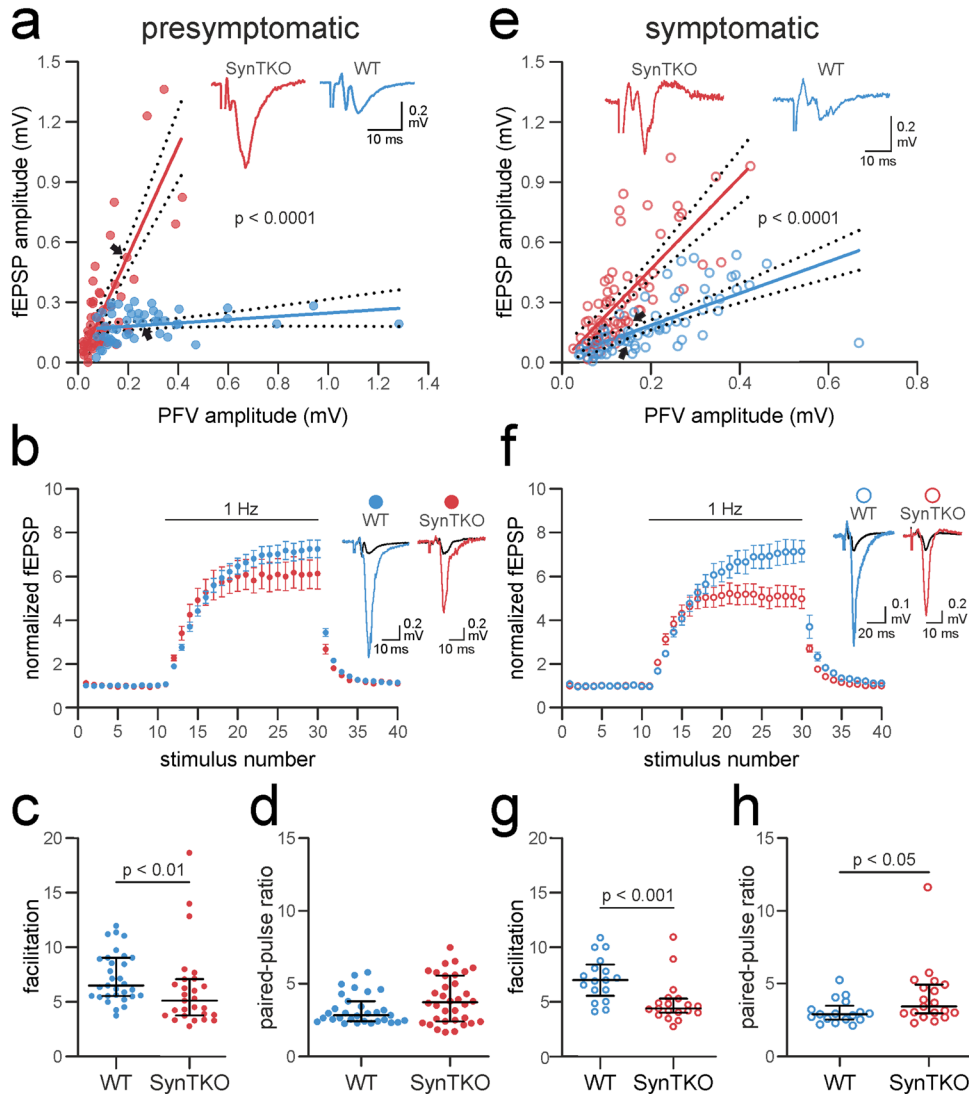


Figure 1. Increased excitability, but reduced facilitation, at mossy fibers of presymptomatic and symptomatic SynTKO mice. **a**, Excitability was increased in brain slices from presymptomatic SynTKO mice (red, 37 slices from 13 animals) compared with WT mice (blue, 31 slices from 12 animals). Pooled fEPSP amplitudes (mV) were plotted against pooled PFV amplitudes (mV) and fitted with a simple linear regression. The slopes of the linear regressions were significantly different ($p < 0.0001$, tested with a two-tailed ANCOVA). The 95% confident bands are shown as dotted lines around the fit. The black arrows indicate the data points corresponding to the example traces shown in the inset. Inset, Example traces from WT (blue) and SynTKO (red) slices with similar PFV amplitudes. Note the difference in the corresponding fEPSP amplitude. **b, c**, Frequency facilitation is reduced in presymptomatic SynTKO (red) compared with WT (blue) slices. **b**, Averaged normalized fEPSP amplitudes \pm SEM from all WT (blue, 31 slices from 12 animals) and SynTKO (red, 27 slices from 9 animals) recordings plotted against the number of stimuli. Stimuli 1–10 were given with a frequency of 0.05 Hz, Stimuli 11–30 with 1 Hz, and Stimuli 31–41 with a frequency of 0.05 Hz again. Both time and the interaction between genotype and time were significantly different in a mixed-effect model ($p < 0.0001$; $p < 0.001$). Post hoc Sidak’s test for multiple comparisons revealed no significant differences. Right, Example fEPSP amplitudes from WT (blue) and SynTKO (red) recordings at the 20th 1 Hz stimulus. Respective baseline fEPSP amplitudes are shown in black. **c**, fEPSP amplitudes at the 20th stimulus at 1 Hz for individual WT (blue dots; 31 slices from 12 animals) and SynTKO (red dots; 27 slices from 9 animals) recordings. Median values \pm interquartile ranges are shown in black. Facilitation was significantly different ($p = 0.0089$; Mann–Whitney U test). **d**, PPR for presymptomatic SynTKO and age-matched control animals. Dots represent PPR from individual recordings from WT (blue dots, 31 slices from 12 animals) and SynTKO (red dots, 34 slices from 12 animals) slices, calculated as the ratio of second to first fEPSP amplitude. The interstimulus interval was 50 ms. Median values \pm interquartile ranges are depicted in black. Ranks were compared in a Mann–Whitney U test and were not significantly different ($p = 0.133$). **e**, Excitability was increased in recordings from symptomatic SynTKO mice (red; 18 slices from 5 animals) compared with WT mice (blue; 17 slices from 4 animals). Pooled fEPSP amplitudes (mV) were plotted against pooled PFV amplitudes (mV) and fitted with a simple linear regression. The slopes of the linear regressions were significantly different ($p < 0.0001$, tested with a two-tailed ANCOVA). The 95% confidence bands are shown as dotted lines around the fit. Inset, Example traces from WT (blue) and SynTKO (red) animals with similar PFV amplitudes. Note the difference in the corresponding fEPSP amplitude. **f, g**, Frequency facilitation was reduced in symptomatic SynTKO (red) compared with WT (blue) animals. **f**, Averaged normalized fEPSP amplitudes \pm SEM from all WT (blue; 17 slices from 4 animals) and SynTKO (red; 19 slices from 5 animals) recordings plotted against the number of stimuli. Stimuli 1–10 were given with a frequency of 0.05 Hz, Stimuli 11–30 with 1 Hz, and Stimuli 31–41 with a frequency of 0.05 Hz again. Both time and the interaction between genotype and time were significantly different in a mixed-effect model ($p < 0.0001$). Post hoc Sidak’s test for multiple comparisons revealed significant differences ($p < 0.05$) for two time points. Right, Example fEPSP amplitudes from WT (blue) and SynTKO (red) animals at the 20th 1 Hz stimulus. Respective baseline fEPSP amplitudes are shown in gray. **g**, fEPSP amplitudes at the 20th stimulus at 1 Hz for individual WT (blue dots, 17 slices from 4 animals) and SynTKO (red dots, 19 slices from 5 animals) recordings. Median values \pm interquartile ranges are shown in black. Facilitation was significantly different

design was aimed at differentiating changes in synaptic transmission that could lead to or result from epilepsy in SynTKO animals.

We conducted field recordings in acute slices from SynTKO and WT age-matched controls and recorded the input–output relationship as a measure of synaptic strength. We recorded from the *stratum lucidum* of area CA3 while stimulating close to the granule cell layer in the hilus. We found that SynTKO were significantly more excitable than WT animals: the input–output relation was increased in both 4–6 weeks old (Fig. 1a) and 17–19 weeks old animals (Fig. 1e). With the same amount of stimulated fibers (size of the PFV), the fEPSP amplitudes were larger. The slopes of the simple linear regression fits of fiber volley versus fEPSP amplitudes were significantly different with $p < 0.0001$ between control and SynTKO data for both age groups. For presymptomatic recordings, the slopes for the simple linear regression with 95% confidence intervals were 0.083 [0.005–0.171] for WT and 2.743 [2.159–3.326] for SynTKO and for symptomatic recordings 0.795 [0.59–0.99] for WT and 2.292 [1.806–2.777] for SynTKO.

Changes at the network level, morphological changes, or changes in release probability could underlie this increased excitability. At the network level, this could be explained by the fact that the lack of synapsins differentially affects excitatory and inhibitory neurons (Farisello et al., 2013). Morphology was described to be similar between WT and SynTKO animals (Gitler et al., 2004); therefore we assume that the number of excitable fibers is comparable. To check for a possible change in release probability, we measured the PPR with an interstimulus interval of 50 ms. Under our experimental conditions, the PPR was not significantly different between presymptomatic SynTKO and WT animals (Fig. 1d). In WT recordings, the median PPR was 2.827 [2.423; 3.795], while in recordings from SynTKO, it was 3.745 [2.422; 5.570] ($p = 0.133$; Mann–Whitney U test). However, we saw a trend for an increased PPR that became clearer with a shortening of the interstimulus interval to 40 ms (see first two fEPSPs in Fig. 2a,b). Here, in WT recordings, the median PPR was 2.91 [2.654; 4.026], while it was 4.436 [3.485; 6.094] for SynTKO. The p value was 0.07 (Mann–Whitney U test). Finally, in symptomatic SynTKO animals, the PPR was significantly increased compared with WT animals with $p = 0.03$ (Mann–Whitney U test) with a median of 2.906 [2.549; 3.499] for WT and 3.435 [2.964; 4.944] for SynTKO animals (Fig. 1h). A change in PPR is suggestive of a change in release probability (Dobrunz and Stevens, 1997); however, this might be taken with caution as many other factors affect this measure (Hanse and Gustafsson, 2001; H. Y. Sun et al., 2005; Neher and Brose, 2018; Glasgow et al., 2019).

Reduced frequency facilitation in mossy fibers of SynTKO animals

Mossy fiber boutons are very powerful synapses when it comes to presynaptic plasticity. They are able to facilitate dramatically, even at moderate frequencies (Salin et al., 1996). This phenotype, together with large pools of synaptic vesicles (Hallermann et al., 2003; Rollenhagen et al., 2007), makes them an excellent system for studying the influence of synapsins on presynaptic plasticity. In previous work, it has been reported that frequency facilitation is impaired at mossy fibers from SynDKO animals after stimulation with a moderate frequency of 2 Hz (Owe et al., 2009). The authors suggested that the remaining synapsin isoform—SynIII—causes impaired facilitation since it was localized in the RRP of mossy fiber boutons. Additionally, neurons from SynIII KO animals show less synaptic depression than WT neurons in primary hippocampal cultures (Feng et al., 2002). Here, we intended to test if complete deletion of synapsins, including SynIII, would rescue frequency facilitation at the hippocampal mossy fiber bouton.

When stimulated with a train of 20 pulses at a frequency of 1 Hz, we saw less facilitation in mossy fibers from presymptomatic SynTKO compared with WT animals. This finding is comparable to the aforementioned experiments in SynDKO animals (Owe et al., 2009) and cell culture experiments of SynTKO animals (Gitler et al., 2004). The rise in the field excitatory postsynaptic potential (fEPSP) amplitudes was similar in WT and SynTKO during the first 10 stimuli, but in SynTKO animals we observed an earlier saturation of amplitudes (Fig. 1b). When comparing the plots with a mixed-effects model, we found significant differences for the factor time ($p < 0.0001$), as well as for the interaction between time and genotype ($p < 0.001$). The post hoc Sidak's test for multiple comparisons revealed no significant differences for single time points ($p > 0.05$). When comparing the amplitudes in response to the last 1 Hz stimulus, we found that the median facilitation was 6.52 [5.553; 9.047] for WT animals, while the increase was only 5.110 [3.76; 7.08] compared with the baseline for SynTKO animals [median value (25% quartile; 75% quartile)]. Ranks were different with $p = 0.0089$ [Mann–Whitney U test (Fig. 1c)].

All synapsin KO animals lacking SynI and/or SynII develop seizures beginning at the age of two months (Fassio et al., 2011) that could potentially lead to secondary differences in plasticity. We therefore investigated short-term plasticity also in 17–19-week-old symptomatic mice—matching the age range from Owe et al. (2009). In symptomatic mice, we observed a more pronounced effect on frequency facilitation (Fig. 1f,g): the facilitation in WT animals reached 7.019 [5.574; 8.440], while the increase in SynTKO recordings was only 4.414 [4.036; 5.330] compared with the baseline [median (25% quartile; 75% quartile)]. Ranks were significantly different with $p = 0.0009$ (Mann–Whitney U test). In summary, we see a decrease in

←
($p = 0.0009$; tested with Mann–Whitney U test). **h**, PPR for symptomatic SynTKO and age-matched control animals. Top, Example traces for a paired-pulse from WT (dark blue) and SynTKO (dark red) recordings, respectively. Bottom, Dots represent PPR from individual recordings from WT (dark blue dots, 17 slices from 4 animals) and SynTKO (dark red dots, 19 slices from 5 animals) slices, calculated as the ratio of second to first fEPSP amplitude. The interstimulus interval was 50 ms. Median values \pm interquartile ranges are depicted in black. Ranks were compared in a Mann–Whitney U test and were significantly different ($p = 0.0325$).

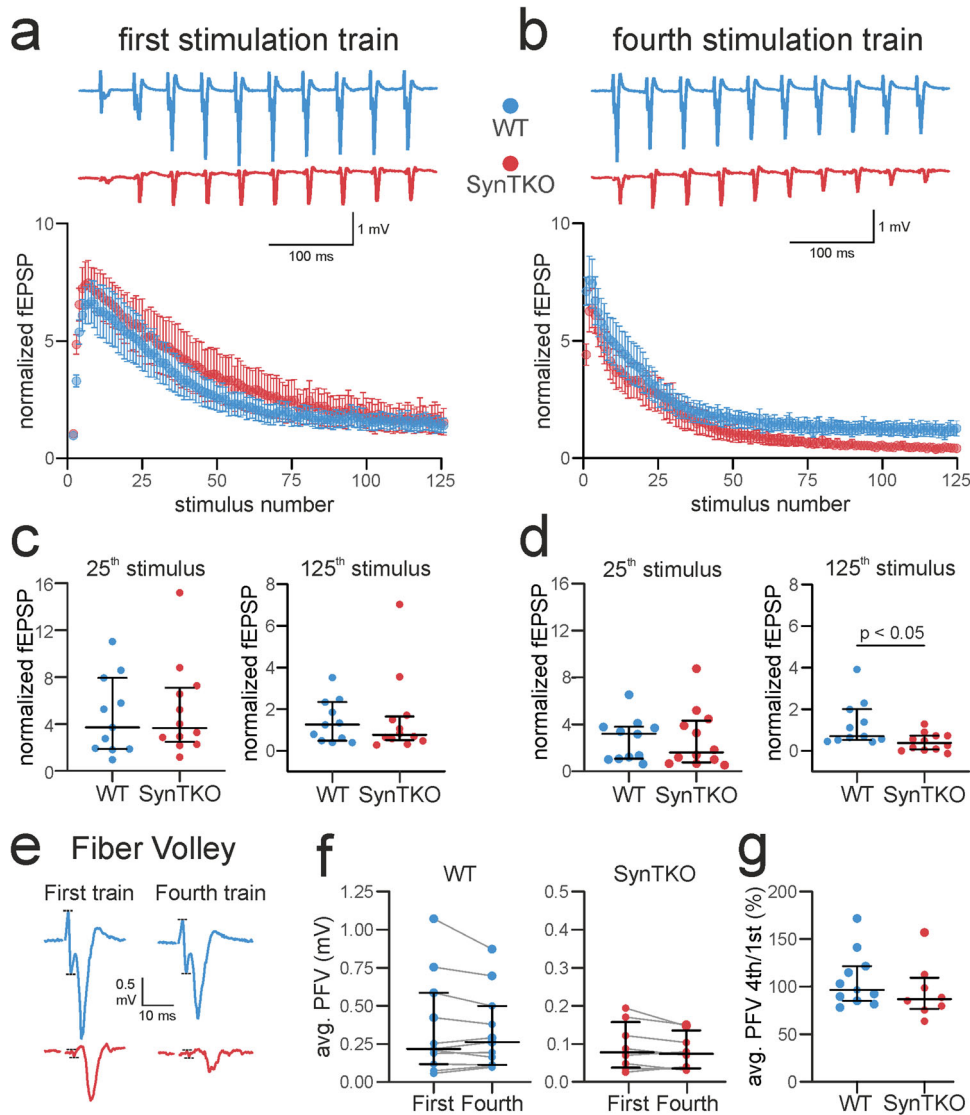


Figure 2. Faster depression during high-frequency stimulation in SynTKO mice. High-frequency stimulation comprised four trains of 125 pulses at 25 Hz with an interval of 20 s between the first stimuli of consecutive trains. **a**, Top, Example traces show fEPSP amplitudes of mossy fibers from WT (blue) and SynTKO (red) slices in response to the first 10 stimuli of the first high-frequency stimulation train. Bottom, Normalized averaged fEPSP amplitudes plotted against the number of stimuli of the first high-frequency stimulation train for WT (blue, 11 slices from 5 animals) and SynTKO (red, 12 slices from 6 animals) recordings. A mixed-effect model revealed no significant difference between genotypes ($p = 0.59$), but significant differences ($p < 0.0001$) for the factor time (stimulus). A post hoc Sidak's test for multiple comparisons revealed no significant differences for single time points. **b**, Top, Example traces show fEPSP amplitudes of WT (blue) and SynTKO (red) animals in response to the first 10 stimuli of the fourth high-frequency stimulation train. Bottom, Normalized averaged fEPSP amplitudes plotted against number of stimuli of the first high-frequency stimulation train for WT (blue, 11 slices from 5 animals) and SynTKO (red, 12 slices from 6 animals) animals. The factor time (stimulus) was significantly different in a mixed-effect model ($p < 0.0001$), while the genotype and the interaction of both were not ($p = 0.22$ and $p > 0.99$). A post hoc Sidak's test for multiple comparisons revealed no significant differences for single time points. **c**, Normalized fEPSP amplitudes at the 25th and 125th stimulus of the first stimulation train for individual WT (blue dots, 11 slices from 5 animals) and SynTKO (red dots, 12 slices from 6 animals) recordings. Median values \pm interquartile ranges are shown in black. Ranks were not significantly different for either 25th ($p = 0.695$; Mann-Whitney U test) or 125th stimulus ($p = 0.74$, Mann-Whitney U test). **d**, Normalized fEPSP amplitudes at the 25th and 125th stimulus of the fourth stimulation train for individual WT (blue dots, 11 slices from 5 animals) and SynTKO (red dots, 12 slices from 6 animals) recordings. Median values \pm interquartile ranges are shown in black. Ranks were significantly different at the 125th stimulus ($p = 0.032$; Mann-Whitney U test), but not at the 25th stimulus ($p = 0.88$; Mann-Whitney U test). **e**, The loss of fibers during high-frequency stimulation is not substantial and similar for SynTKO and WT mice. Exemplary traces from high-frequency stimulation trains for WT (blue) and SynTKO (red) animals. The 10th PFV and fEPSP from the first and fourth stimulation train are depicted, respectively. Dotted lines indicate the peaks of the PFV. Note that although the PFV is smaller for SynTKO (due to technical reasons in response to the high excitability), the size is relatively consistent throughout the trains. **f**, Averaged PFV (mV) taken from 10–15 pulses from the first and fourth stimulation train, respectively, for recordings from WT (blue, 11 slices from 5 animals) and SynTKO (red, 12 slices from 6 animals) slices. Average values from the same recording are connected. Median values and interquartile ranges are depicted in black. Ranks between first and fourth stimulation train were not significantly different for neither WT ($p = 0.36$) nor SynTKO ($p = 0.08$) recordings, compared in a Wilcoxon test. **g**, The relative loss of fibers was similar for WT and SynTKO recordings. Averaged ratios between fourth and first train PFV sizes are depicted for both WT (blue, 11 slices from 5 animals) and SynTKO (red, 12 slices from 6 animals) animals. Median values and interquartile ranges are depicted in black. Ranks were not significantly different ($p = 0.24$) in a Mann-Whitney U test.

frequency facilitation but an increase in excitability in SynTKO animals. These results indicate that (1) the presence rather than the absence of specific synapsin isoforms is needed to rescue facilitation and (2) excitability and short-term plasticity mechanisms are already altered before the onset of epileptic seizures.

High-frequency stimulation leads to early vesicle exhaustion in SynTKO animals

Since stimulation with a moderate frequency led to a decrease in facilitation in presymptomatic SynTKO animals (Fig. 1*b,c*), we wanted to investigate the response to a longer stimulation with a higher frequency. We applied four trains of 125 pulses at 25 Hz. While the course of the amplitudes was very similar in the first high-frequency train for both genotypes (Fig. 2*a,c*), changes manifested over time. Differences between WT and SynTKO animals became distinguishable in the fourth stimulation train (Fig. 2*b,d*) with smaller amplitudes towards the end of the train in SynTKO animals.

When tested with a mixed-effects model, we detected significant differences for the factor time (stimuli) for both the first and the fourth stimulation train ($p < 0.0001$). A post hoc Sidak's test for multiple comparisons revealed no significant differences for single time points for either of the stimulation trains. We also compared the amplitudes for the 25th and 125th stimulus of the stimulation trains between genotypes. Ranks were comparable between genotypes in the first stimulation train at the 25th and 125th stimulus as well as at the 25th stimulus of the fourth stimulation train (Table 7). However, when comparing the amplitudes of the 125th stimulus of the fourth stimulation train, we found a significant difference ($p = 0.032$, Mann–Whitney U test) between WT and SynTKO (Fig. 2*a*). Here, the median normalized fEPSP amplitude was 0.687 [0.501; 1.987] for WT and 0.3714 [0.049; 0.72] for SynTKO animals. This stronger exhaustion during intense stimulation was already described before in other synapsin KO animals (Rosahl et al., 1995; Farisello et al., 2013) and probably reflects the missing reserve pool, which would normally replenish the RRP under such high activity (Vasileva et al., 2012).

High-frequency stimulation can lead to a loss of fibers during the course of stimulation. To check if the smaller fEPSP amplitudes in the last stimulation train of SynTKO recordings are due to an increased fiber loss, we measured a subset of the PFVs during the first and fourth stimulation train for both genotypes, respectively. While PFVs of SynTKO animals were in general smaller than the ones from WT animals with comparable fEPSP amplitudes (Fig. 1*a*), there was no relative difference in PFV sizes of the two genotypes between first and last stimulation train (Fig. 2*e–g*). Thus, we conclude that the relative loss of fibers is similar for both genotypes and does not explain the more drastic decrease in the fEPSP size for SynTKO animals.

Here, our data indicate that deletion of all synapsins disturbs vesicle organization in synaptic terminals in a way that leads to impaired replenishment. This is especially relevant for synapses like mossy fiber boutons, which have large vesicle pools (Hallermann et al., 2003; Rollenhagen et al., 2007).

PTP is changed in SynTKO animals

After intense stimulation of mossy fibers, PTP (Griffith, 1990), another form of short-term plasticity, occurs, which was proposed to underlie short-term memory (Vandael et al., 2020). Measuring PTP after four trains of high-frequency stimulation revealed differences between WT and SynTKO animals: while in WT recordings the median potentiation was 7.229 [5.701; 8.464]-fold compared with the baseline and decreased over time, in SynTKO recordings, we initially measured an amplitude which was only 3.702 [2.683; 5.280] times larger than the baseline (significantly different in a Kruskal–Wallis test with post hoc Dunn's test for multiple comparisons; $p = 0.0003$) but increased over time. After 1 min, the amplitudes of WT and SynTKO recordings were comparable (Fig. 3*a,b*; WT, 5.323 [4.070; 6.03]; SynTKO, 4.887 [3.769; 6.419]; $p > 0.99$), followed by a further increase in the SynTKO amplitudes over WT amplitudes. One minute after stimulation, the amplitudes of the SynTKO animals remained on a plateau, while the amplitudes in the WT animals decreased further (Fig. 3*a,b*), leading to median amplitudes of 2.749 [2.432; 3.321] for WT and 4.865 [3.635; 6.497] for SynTKO animals ~3 min after

Table 7. Normalized averaged fEPSP amplitudes during high-frequency stimulation at 25 Hz

Train	Measure	WT animals	SynTKO animals
First train 25th stimulus	Median	3.704	3.653
	Interquartile range	[1.873; 7.935]	[2.426; 7.092]
	p value (Mann–Whitney U test)		$p = 0.695$
First train 125th stimulus	Median	1.243	0.7514
	Interquartile ranges	[0.473; 2.332]	[0.4997; 1.650]
	p value (Mann–Whitney U test)		$p = 0.74$
Fourth train 25th stimulus	Median	3.176	1.61
	Interquartile ranges	[1.039; 3.77]	[0.75; 4.314]
	p value (Mann–Whitney U test)		$p = 0.88$
Fourth train 125th stimulus	Median	0.687	0.3714
	Interquartile ranges	[0.501; 1.987]	[0.049; 0.72]
	p value (Mann–Whitney U test)		$p = 0.032$

Amplitudes were measured in both genotypes in the first and fourth train of 125 pulses at 25 Hz (Fig. 2) at the 25th and 125th stimulus, and their ranks were compared in Mann–Whitney U tests.

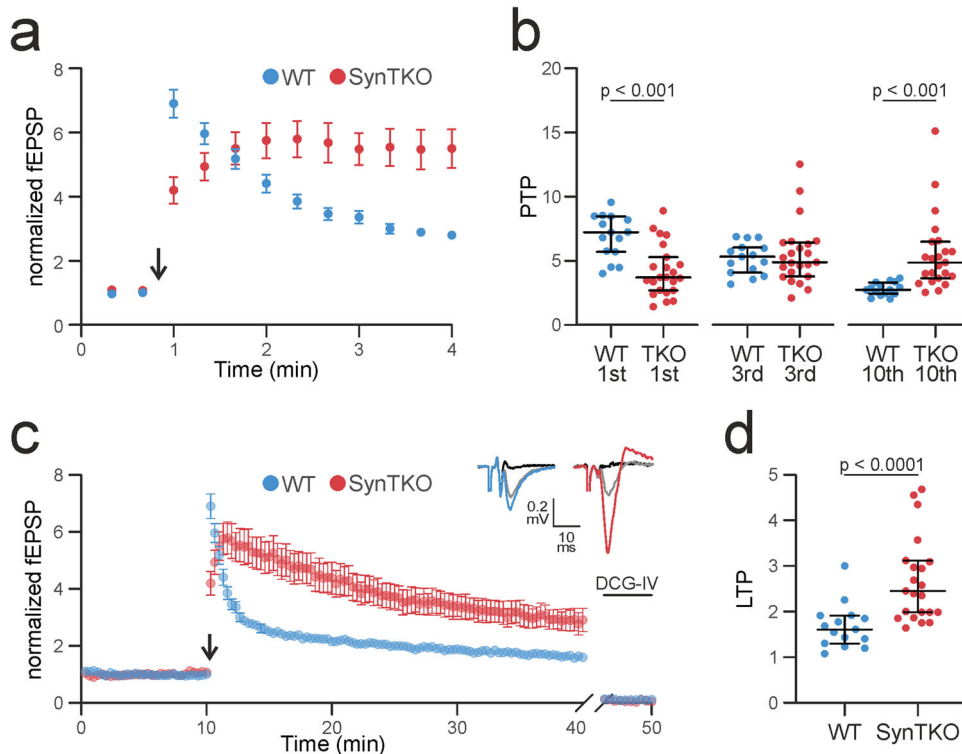


Figure 3. SynTKO mossy fibers display reduced post-tetanic potentiation but increased long-term potentiation. **a**, Post-tetanic potentiation is decreased in SynTKO mossy fibers. Normalized averaged fEPSP amplitudes plotted against time (min) from WT (blue, 15 slices from 6 animals) and SynTKO (red, 23 slices from 9 animals) recordings. This plot is a partial zoom-in from the plot shown in **c** (9–13 min). Mean values \pm SEM are shown. The arrow indicates the time point of high-frequency stimulation (4 times 125 pulses at 25 Hz). Stimulation before and after was at 0.05 Hz. Statistics for dataset as reported in **c**. **b**, Scatterplots for individual fEPSP amplitudes for WT (blue) and SynTKO (red) recordings for the 1st, 3rd, and 10th stimulus after high-frequency stimulation, respectively. Median values \pm interquartile ranges are shown in black. The significance was tested with a Kruskal–Wallis test and a post hoc Dunn’s correction for multiple comparisons. The Kruskal–Wallis test revealed significant differences between ranks with $p < 0.0001$. Multiple comparisons revealed significant differences for the 1st ($p = 0.0003$) and 10th ($p = 0.0002$) time point. **c**, LTP is increased in SynTKO animals after 30 min. Top, Example traces of fEPSP amplitudes 30 min after high-frequency stimulation for mossy fibers from WT (blue, left) and TKO (red, right) mice compared with baseline fEPSP amplitude (gray) and response to 1 μ M DCG-IV (black). Bottom, Normalized averaged fEPSP amplitudes plotted over time (min) from WT (blue, 15 slices from 6 animals) and SynTKO (red, 23 slices from 9 animals) recordings. Mean values \pm SEM are shown. The arrow indicates the high-frequency stimulation (4 times 125 pulses at 25 Hz). Stimulation frequency before (baseline) and after (LTP recording) was 0.05 Hz. At the end of the recording, 1 μ M DCG-IV was washed in to ensure mossy fiber specificity. The last 10 fEPSP amplitudes during DCG-IV wash-in are shown at the end of the recording. A mixed-effect model revealed significant differences for the genotype ($p = 0.005$), time ($p < 0.0001$), and the interaction of both ($p < 0.0001$). A post hoc Sidak’s test for multiple comparisons revealed significant differences for the first sweep after high-frequency stimulation ($p = 0.0125$) and Sweeps 38 ($p < 0.05$) and Sweeps 40–54 ($p < 0.05$; ~14–18 min), as well as for Sweeps 61, 67, and 94 ($p < 0.05$; ~20, 22, and 32 min). **d**, Dots indicate averaged fEPSP amplitudes from individual WT (blue) and SynTKO (red) recordings. Amplitudes were averaged over the last 10 min of the LTP recording; from 20 to 30 min after high-frequency stimulation. Median values \pm interquartile ranges are shown in black. Ranks were significantly different with $p < 0.0001$ (Mann–Whitney U test).

high-frequency stimulation (significantly different with $p = 0.0002$). These findings point to different underlying mechanisms: one leading to the impairment of PTP right after high-frequency stimulation and another one leading to increased amplitudes after some recovery time and upon low-frequency stimulation of 0.05 Hz. To understand this observation further, we continued recording for half an hour, which corresponds to early LTP.

LTP is enhanced in SynTKO animals

Mossy fiber boutons express a presynaptic form of LTP, which is PKA-dependent (Weisskopf et al., 1994). In recordings from SynDKO animals, mossy fiber LTP was unchanged compared with WT animals (Spillane et al., 1995). It is tempting to speculate, though, that SynIII might be the phosphorylation target of PKA in the context of LTP, since a PKA phosphorylation site is present in domain A (Piccini et al., 2015), which is conserved among all synapsins, and SynIII expression is maintained in adult mossy fiber boutons (Pieribone et al., 2002). A complete loss of synapsins could therefore lead to a block of LTP. However, when recording LTP (Fig. 3c), we measured a median potentiation of 1.6 [1.3; 1.92] in WT animals 20–30 min after the high-frequency stimulation, while SynTKO animals showed a larger median potentiation of 2.45 [1.98; 3.12] compared with the baseline (Fig. 3a). Ranks differed significantly with $p < 0.0001$ (Mann–Whitney U test). The time course of LTP was tested in a mixed-effects model. The factors genotype, time, and the interaction of both differed

significantly ($p < 0.0001$; $p = 0.005$; $p < 0.0001$, respectively). A post hoc Sidak's test for multiple comparisons revealed significant differences for single time points as well (Fig. 3c legend). We included all measurements that fulfilled the specificity criterion, which was tested by the application of the metabotropic glutamate receptor group II agonist DCG-IV (Kamiya et al., 1996; last 10 sweeps are shown in Fig. 3c).

In summary, the absence of all synapsin isoforms in mossy fiber synapses leads to a reduced early PTP, an altered time course of PTP/LTP and an increased long-lasting potentiation. Such changes in LTP have not been described before in other synapsin KO models, suggesting that this effect is specifically relevant for the mossy fiber bouton, where LTP occurs presynaptically (Zalutsky and Nicoll, 1990) and only present upon the complete loss of synapsins. Since it has been shown that ultrastructural changes underlie potentiation at hippocampal mossy fibers (Orlando et al., 2021), we next sought to investigate the ultrastructure of mossy fiber boutons in SynTKO animals.

Synaptic vesicles are more dispersed in SynTKO animals

So far, vesicle distributions at the hippocampal mossy fiber bouton have only been described for either SynDKO animals or SynIII KO animals (Feng et al., 2002; Owe et al., 2009). Here, we wanted to test whether the KO of all three synapsins would lead to additional changes in vesicle organization at the hippocampal mossy fiber bouton. Using TEM, we identified individual mossy fiber boutons from three presymptomatic SynTKO and three age-matched WT mice. We imaged serial sections from 16 SynTKO and 18 WT mossy fiber boutons. For each 2D projection, we measured the vesicle number and the MNND using an automated tool (Imbrosci et al., 2022; Fig. 4). For both datasets, we used a generalized linear mixed model to estimate either the vesicle density or MNND. When comparing synaptic vesicles of WT and SynTKO boutons, the median density was strongly reduced in boutons from SynTKO animals (702.5 [499; 882.9] vesicles/ μm^3 compared with 2,102 [1,861; 2,916] vesicles/ μm^3 in WT; Fig. 4b,c). In a hypothesis test between nested models, the genotypes were

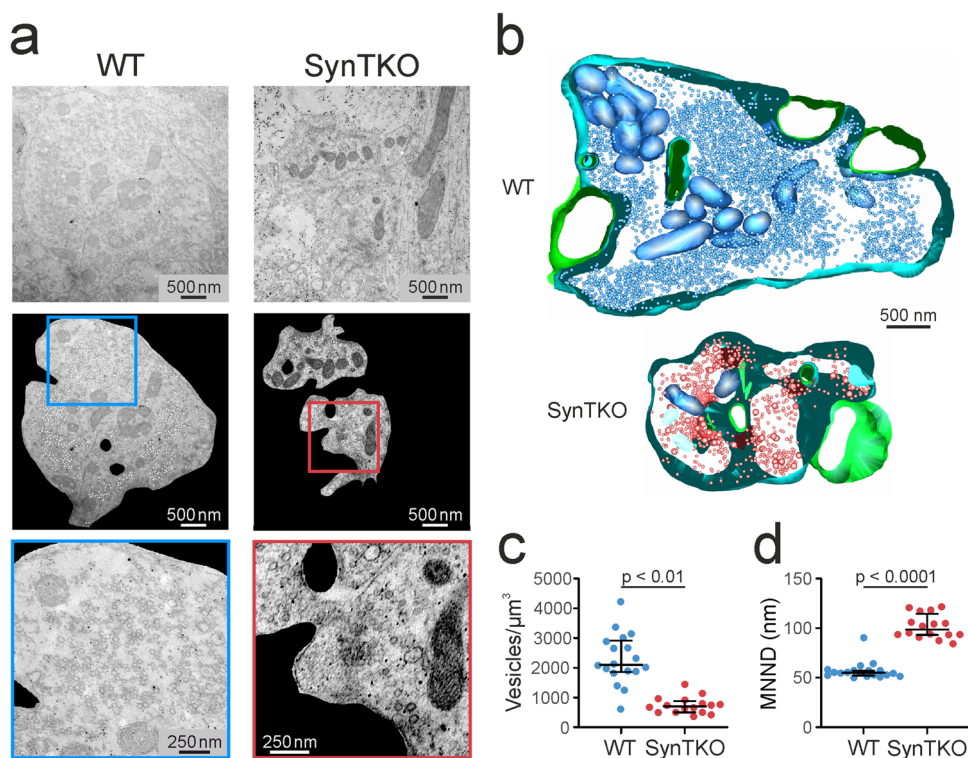


Figure 4. Synaptic vesicles are more dispersed in mossy fiber boutons from SynTKO mice. **a**, In mossy fiber boutons, synaptic vesicles are more dispersed, and their density is reduced. Example images from TEM showing mossy fiber boutons from WT (left) and SynTKO (right) animals. Top, Raw TEM images of mossy fiber boutons in stratum lucidum. Middle, An automated tool (Imbrosci et al., 2022) was used to detect vesicles. Mossy fiber boutons were extracted from the raw image, and the center of detected vesicles is marked with a white dot. Blue and red boxes show the region for the zoom-ins in WT and SynTKO, respectively. Bottom, Zoom-ins, as marked in the middle pictures. High-magnification images of mossy fiber boutons from a WT and a SynTKO animal, respectively. Note the reduced abundance of synaptic vesicles in the SynTKO bouton. **b**, Partial 3D reconstruction of hippocampal mossy fiber boutons from a WT (top) and a SynTKO animal (bottom) for visualization purposes only. Vesicles are shown in blue and red, respectively, the presynaptic mossy fiber membrane is shown in light blue, and postsynaptic spines are shown in green. **c**, The number of synaptic vesicles per cubic micrometer is reduced in SynTKO animals. Dots represent the number of vesicles in individual mossy fiber boutons from three WT (blue, 18 boutons) and three SynTKO (red, 16 boutons) animals. Median values and interquartile ranges are shown in black. A generalized linear mixed model revealed significant differences between genotypes with $p = 0.0015$. **d**, The MNND is increased between synaptic vesicles in SynTKO compared with those in WT boutons. The scatterplot shows average MNND (nm) for individual mossy fiber boutons from three WT (blue, 18 boutons) and three SynTKO (red, 16 boutons) animals. Genotypes were significantly different in a generalized linear mixed model with $p = 0.0015$. Median values are shown in black with interquartile ranges.

significantly different with $p = 0.0015$. Consequently, we also saw an increase in the MNND of vesicles (Fig. 4b,d): the median MNND was 55.05 [52.24; 57.28] nm for WT and 98.58 [93.38; 114.4] nm for SynTKO boutons. Groups were significantly different with $p = 0.0015$. The reduced density of distal vesicles implies a reduced reserve pool. Since this observation resembles the results seen in mossy fiber boutons of SynDKO animals (Owe et al., 2009), our data indicate that the additional KO of SynIII does not add on effects on the organization of the distal pool. This conclusion is also in line with unchanged synaptic vesicle densities in mossy fiber boutons of SynIII KO mice (Feng et al., 2002).

Together, our data confirm a reduced distal vesicle pool, as it had been described before in cultured SynTKO and SynDKO mossy fibers (Spillane et al., 1995; Siksou et al., 2007).

Active zone density is highest in chemically potentiated mossy fiber boutons from SynTKO animals

Since we saw an increase in LTP in SynTKO animals (Fig. 3c,d), we wanted to understand if structural changes would occur in potentiated mossy fiber boutons from SynTKO animals. We performed TEM in hippocampal slices from young WT and presymptomatic SynTKO animals in either potentiated or control conditions. Potentiation was chemically induced via incubation with the adenylyl cyclase-activator FSK before fixation of the samples. FSK induces an increase in intracellular cAMP and has similar effects on mossy fibers as high-frequency electrical stimulation (Weisskopf et al., 1994; Spillane et al., 1995). Structural measures following potentiation included bouton complexity, active zone density, active zone area, and docked synaptic vesicle density. We estimated bouton complexity as the ratio between perimeter and area of each presynaptic profile in 2D images from three animals per group. The median complexity was similar between control and chemically potentiated boutons of both WT and SynTKO animals [median value (interquartile range) for WT: 2.61 [2.29; 3.35] μm^{-1} , for WT + FSK: 2.65 [2.13; 3.43] μm^{-1} , for SynTKO: 3.24 [2.69; 4.09] μm^{-1} and for SynTKO + FSK: 4.25 [3.93; 5.25] μm^{-1} ; Fig. 5d]. A hypothesis test between nested generalized linear mixed models revealed no significant differences ($p = 0.3972$).

The active zone density was analyzed in partial 3D reconstructions of mossy fiber boutons as the measure of the total number of reconstructed active zones (see Materials and Methods for details) normalized by the volume of the reconstructed bouton (μm^3). We fitted a generalized linear mixed model to estimate active zone density given the genotype and FSK treatment. We found a significant difference for FSK treatment ($p < 0.001$) when we compared the model with the respective null model. Specific pairs were compared by testing estimated marginal means with adjustment for the false discovery rate (Benjamini and Hochberg, 1995).

We observed a significant increase ($p = 0.0134$) in the active zone density in WT animals when treated with FSK, as described before (Orlando et al., 2021). Untreated boutons from SynTKO animals had a similar mean density of active zones as FSK-treated boutons from WT animals (5.63 [4.43; 7.14] active zones/ μm^3 for untreated SynTKO boutons; 5.22 [4.13; 6.60] active zones/ μm^3 for FSK-treated WT boutons, $p = 0.658$). This indicates that, from a structural point of view, SynTKO animals could be in a similar state as potentiated WT boutons. Treatment with FSK led to a further increase in the active zone density in mossy fiber boutons from SynTKO animals (10.20 [7.50; 13.88] active zones/ μm^3 ; Fig. 5a,b) and led to significant differences when compared with untreated SynTKO boutons ($p = 0.0018$) as well as treated WT boutons ($p = 0.0018$; Fig. 5e).

Our previous work revealed that the FSK-induced structural changes were not accompanied by a change in the active zone area of mossy fiber boutons (Orlando et al., 2021). To test if this holds true in SynTKO animals, we analyzed the area of individual active zones from partial 3D reconstructions of treated and untreated WT and SynTKO animals. Mean active zone areas per bouton were comparable for both genotypes and treatments (Fig. 5f), with median areas of 0.13 [0.08; 0.22] μm^2 for WT, 0.1 [0.07; 0.16] μm^2 for WT + FSK, 0.15 [0.1; 0.2] μm^2 for SynTKO, and 0.13 [0.09; 0.17] μm^2 for SynTKO + FSK. We fitted a generalized linear mixed model to estimate the active zone area given the genotype and treatment. When comparing the model to a nested null model, we found no evidence for a significant difference between models ($p = 0.8112$), indicating no differences in the active zone areas.

RRP correlate increases in chemically potentiated SynTKO mossy fiber boutons

Finally, we wanted to assess if the number of docked vesicles would change depending on the genotype or treatment. While chemical fixation is not ideal for the analysis of this parameter, our analysis allows us to get an idea of potential changes in the number of docked vesicles. We analyzed the number of docked vesicles per 3D reconstruction and normalized the total number to the respective bouton volume. The docked synaptic vesicle density was slightly increased from control to FSK-treated WT boutons with a median density of 85.36 [56.39; 108.8] synaptic vesicles/ μm^3 for WT and 89.75 [57.54; 145.1] synaptic vesicles/ μm^3 for WT + FSK. In contrast, the docked synaptic vesicle density increased in FSK-treated SynTKO boutons when compared with that in untreated SynTKO: the median density was 125.5 [65.69; 139.6] synaptic vesicles/ μm^3 for SynTKO and 205.7 [168.8; 270.5] synaptic vesicles/ μm^3 for SynTKO + FSK. We fitted a generalized linear mixed model to estimate the normalized number of docked vesicles given the genotype and treatment. When comparing the model to nested null models, we found a small — not statistically significant — increase in docked vesicles in FSK-treated WT boutons ($p = 0.08$) and a significant effect of FSK treatment on the number of docked vesicles in the SynTKO animals ($p = 0.0009$; Fig. 5g).

Taken together, our data show a structural strengthening in boutons from SynTKO animals: both the RRP correlate and the active zone density (Fig. 5) are increased upon FSK treatment, which might explain the increase in LTP (Fig. 3c,d).

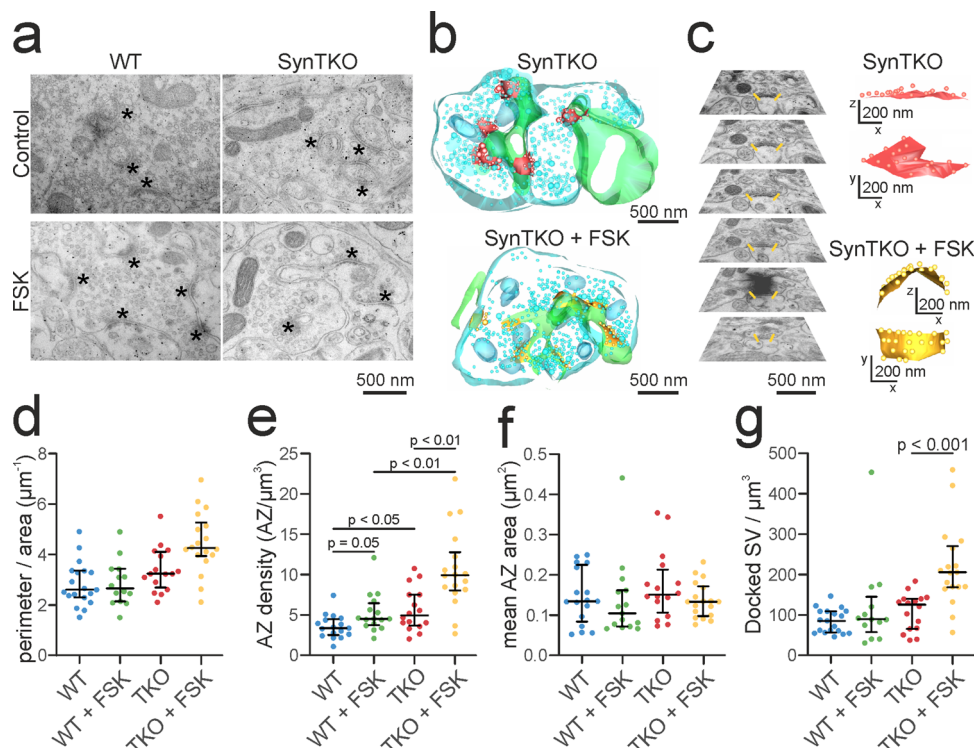


Figure 5. Increased active zone density in mossy fiber boutons of SynTKO mice. **a**, Example images from TEM showing mossy fiber boutons from WT (left) and SynTKO (right) animals in control (top) and FSK (bottom) condition. Black asterisks indicate the active zones. **b**, Example partial 3D reconstructions of mossy fiber boutons from untreated (top) and FSK-treated (bottom) SynTKO mice. Active zones with docked vesicles are shown in red (SynTKO) and yellow (SynTKO + FSK), respectively. Synaptic vesicles, mitochondria, and presynaptic membrane are shown in light blue; the postsynaptic membrane is shown in green. **c**, Single active zones were reconstructed from serial sections of TEM images. Left, An example stack of serial sections for one active zone, indicated by yellow lines at the active zone boundaries. Right, 3D reconstructions of single active zones from untreated (red) and FSK-treated (yellow) SynTKO mice, in side and top view, respectively. The yellow active zone corresponds to the serial images to the left. **d**, Complexity of boutons [measured as perimeter/area (μm^{-1})] plotted for individual mossy fiber boutons from untreated WT (blue dots, 17 boutons from 3 animals) and untreated SynTKO slices (red dots, 16 boutons from 3 animals) as well as for FSK-treated WT (green dots, 16 boutons from 3 animals) and FSK-treated SynTKO slices (yellow dots, 18 boutons from 3 animals). Median values are shown in black with interquartile ranges. A hypothesis test between nested generalized linear mixed models revealed no significant differences ($p = 0.3972$). **e**, The number of active zones per cubic micrometer plotted for individual mossy fiber boutons from untreated WT (blue dots, 17 boutons from 3 animals) and untreated SynTKO slices (red dots, 16 boutons from 3 animals) as well as for FSK-treated WT (green dots, 16 boutons from 3 animals) and FSK-treated SynTKO slices (yellow dots, 18 boutons from 3 animals). Median values are shown in black with interquartile ranges. A hypothesis test between nested generalized linear mixed models revealed significant differences ($p = 0.04$). A post hoc test (marginal contrasts analysis with p value adjustment) revealed significant differences between WT and SynTKO ($p = 0.0359$), WT and WT + FSK ($p = 0.05$), SynTKO and SynTKO + FSK ($p = 0.005$), and WT + FSK and SynTKO + FSK ($p = 0.005$), but no significant difference between WT + FSK and SynTKO ($p = 0.772$). **f**, The mean active zone area (μm^2) per bouton for individual mossy fiber boutons from untreated WT (blue dots, 17 boutons from 3 animals) and untreated SynTKO slices (red dots, 16 boutons from 3 animals) as well as for FSK-treated WT (green dots, 16 boutons from 3 animals) and FSK-treated SynTKO slices (yellow dots, 18 boutons from 3 animals). Median values and interquartile ranges are shown in black. A hypothesis test between generalized linear mixed models revealed no significant differences ($p = 0.8112$). **g**, The number of docked synaptic vesicles per cubic micrometer plotted for individual mossy fiber boutons from untreated WT (blue dots, 17 boutons from 3 animals) and untreated SynTKO slices (red dots, 16 boutons from 3 animals) as well as for FSK-treated WT (green dots, 16 boutons from 3 animals) and FSK-treated SynTKO slices (yellow dots, 18 boutons from 3 animals). Median values are shown in black with interquartile ranges. A hypothesis test between generalized linear mixed models revealed significant differences for FSK treatment ($p = 0.0002$). A post hoc test (marginal contrasts analysis with p value adjustment) revealed significant differences between SynTKO and SynTKO + FSK ($p = 0.0009$).

Discussion

Here, we investigated the role of synapsin in various forms of presynaptic plasticity at a glutamatergic synapse that retains SynIII expression in adulthood. The genetic deletion of SynI, SynII, SynIII, SynII/III, and SynI/II/III has been investigated extensively in culture and in various synapses from different brain regions over the last years (see Table 8 for an overview). Despite the extensive work, hippocampal mossy fiber plasticity of mice lacking all synapsin isoforms was not yet characterized. To fill this knowledge gap, we performed local field recordings and 3D electron microscopy at hippocampal mossy fibers from SynTKO and age-matched WT male mice. The removal of all synapsin isoforms from hippocampal mossy fiber boutons leads to a phenotype that recapitulates previously published data (Table 8): the dispersion of synaptic vesicles out of the bouton and impaired short-term plasticity. The impaired PTP indicates a potential role of synapsins in short-term memory. We additionally observed increased LTP in SynTKO mossy fibers, accompanied by

Table 8. Overview of functional and structural changes in glutamatergic synapses of synapsin KOs

Genotype	Syn I KO	Syn II KO	Syn III KO	SynDKO	SynTKO	References
Excitability		↑			↑ (†)	Boido et al., 2010; Farisello et al., 2013; Matos et al., 2019 (this work)
Frequency facilitation	↓	=		↓	(↓)	Owe et al., 2009; Nikolaev and Heggelund, 2015 (this work)
Depression	=↑	=↑	↑	↑	↑ (†)	Rosahl et al., 1995; Feng et al., 2002; Gitler et al., 2004; J. Sun et al., 2006; Vasileva et al., 2012; Farisello et al., 2013 (this work)
PTP	=↓	=↓		↓	↓ (↓)	Rosahl et al., 1993, 1995; Spillane et al., 1995; Kielland et al., 2006; Valente et al., 2012; Farisello et al., 2013; Nikolaev and Heggelund, 2015; Cheng et al., 2018 (this work)
LTP	=			=	(†)	Rosahl et al., 1993, 1995; Spillane et al., 1995; Takei et al., 1995 (this work)
Density of synaptic vesicles	↓		=	↓	↓(↓)	Li et al., 1995; Pieribone et al., 1995; Rosahl et al., 1995; Takei et al., 1995; Feng et al., 2002; Gitler et al., 2004; Siksou et al., 2007; Owe et al., 2009; Vasileva et al., 2012 (this work)

Arrows indicate an increase or decrease of the properties listed in the first column, while equal signs indicate no changes. Bold symbols indicate that previous work also considered the hippocampal mossy fiber bouton. References are marked accordingly. Arrows in brackets refer to the findings of this study.

an increase in active zone density. Together, our results show that synapsins play a role in the modulation of mossy fiber-specific presynaptic plasticity.

In SynTKO mice, we found increased excitability, measured by a change in the input–output relation of local fEPSPs (Fig. 1). Although many factors can influence this measure, we think that a likely explanation is based on the finding that synapsins play different roles in excitatory versus inhibitory neurons (Song and Augustine, 2015). Deletion or mutation of SynI, SynIII, or all synapsins leads to impaired basal transmission of inhibitory, but not excitatory cultured neurons (Terada et al., 1999; Feng et al., 2002; Gitler et al., 2004; Baldelli et al., 2007). Loss of SynII impairs tonic inhibition in hippocampal slices (Medrihan et al., 2013, 2015) and increases excitability in hippocampal cultured neurons (Matos et al., 2019). Mossy fibers activate at least four times more inhibitory neurons than pyramidal cells in CA3 (Acsády et al., 1998), regulating CA3 excitability via feedforward inhibition (Acsády and Káli, 2007; Torborg et al., 2010). Reduced feedforward inhibition might thus explain the increased excitability. Indeed, the input–output relation is increased in Schaffer collaterals from SynTKO animals, while it is reduced in inhibitory fibers from CA1 (Farisello et al., 2013). Here we recorded extracellular local field potentials and could not address the contributing effects of the lack of synapsin in GABAergic synapses to the network.

During trains of activity, mossy fiber boutons facilitate reliably (Salin et al., 1996; Toth et al., 2000), a feature which is thought to be important for information transfer (Henze et al., 2002; Mori et al., 2004). In mossy fibers from SynDKO animals, frequency facilitation is reduced (Owe et al., 2009). Owe and coworkers suggested that the remaining SynIII may act as a brake on facilitation, because (1) SynIII is associated specifically with the RRP in mossy fiber boutons (Owe et al., 2009) and (2) synaptic depression is reduced in SynIII KO cultures (Feng et al., 2002). However, in animals lacking all synapsins, including SynIII, we still observed reduced frequency facilitation (Fig. 1). Frequency facilitation is most likely calcium-dependent and involves increased neurotransmitter release (Chamberland et al., 2017; Jackman and Regehr, 2017). Hence, potential reasons for reduced facilitation are diverse and include enhanced basal release probability, depletion of the RRP, and saturation of postsynaptic receptors (Neher and Sakaba, 2008).

High-frequency stimulation usually results in a biphasic depression, attributed to the depletion of the RRP (Zucker and Regehr, 2002) and slow replenishment from the reserve pool (Wesseling and Lo, 2002). We observed frequency-dependent depression for both genotypes when stimulating at 25 Hz (Fig. 2) but stronger depression in SynTKO animals, recapitulating previous results in SynTKO cultured neurons (Gitler et al., 2004). At the calyx of Held, a reduced reserve pool and slower replenishment accounted for faster depression in SynTKO animals (Vasileva et al., 2012). Indeed, in mossy fiber boutons of SynTKO animals, vesicles were reduced in density and more dispersed (Fig. 4), likely explaining faster depression. Impaired distal pools were described before for mossy fiber boutons (Takei et al., 1995; Owe et al., 2009) and in neuronal cultures from Syn KOs (Li et al., 1995; Gitler et al., 2004; Siksou et al., 2007), with the exception of SynIII KO mice (Feng et al., 2002; Table 8). Hence, at mossy fibers, the KO of all synapsins recapitulates previously described phenotypes of synaptic vesicle dispersion (Table 8). In general, vesicle declustering and reduced vesicle density likely have diverse effects on the release cycle (Bykhovskaia, 2011), possibly also supporting increased excitability and reduced frequency facilitation.

PTP has recently been suggested to underlie short-term memory. During mossy fiber PTP a “pool engram” is formed, i.e., the number of docked vesicles at active zones increases (Vandael et al., 2020). This engram formation depends on the

refilling rate of vesicles and could thus be mediated by synapsins. In line with this hypothesis, we here show that the complete loss of synapsins impairs mossy fiber PTP significantly (Fig. 3). Reduced PTP was previously observed in synapsin KO models, with diversity regarding synapsin isoform and synapse type. PTP is slightly reduced (1) in mossy fibers of SynDKO mice (Spillane et al., 1995); (2) at Schaffer collaterals of SynI KO, SynII KO, SynDKO, and SynTKO mice (Rosahl et al., 1993, 1995; Farisello et al., 2013); (3) in cultured hippocampal neurons of SynI KO and SynTKO animals (Valente et al., 2012; Cheng et al., 2018); and (4) at corticothalamic synapses of SynI KO and SynDKO, but not SynII, KO animals (Kielland et al., 2006; Nikolaev and Heggelund, 2015). Here, we show a more drastic reduction in the initial PTP as well as an altered time course of PTP (Fig. 3) in comparison with SynDKO animals (Spillane et al., 1995), which leads us to hypothesize that also SynIII plays a role in mossy fiber presynaptic potentiation. Indeed, in cell culture, PTP measured via miniature excitatory postsynaptic currents could only be rescued by the SynIIIa isoform (Cheng et al., 2018). We could not test this hypothesis in this study due to the lack of direct comparison with SynIII knockouts.

We analyzed the density of docked vesicles as an ultrastructural correlate of the RRP and noticed no significant difference between SynTKO and WT mossy fiber boutons (Fig. 5g). Upon FSK treatment, we observed an increase in docked vesicles at SynTKO mossy fibers (Fig. 5g). We found a small (nonsignificant $p = 0.08$) increase in the RRP in WT boutons treated with FSK [in line with high pressure freezing experiments by Orlando et al. (2021) and Kim et al. (2023)]. This modulation of the vesicles close to active zones in SynTKO might indicate that synapsin-independent mechanisms are available at mossy fiber boutons that mobilize vesicles to the RRP upon increase in cAMP levels. Nevertheless, this dataset should not be overinterpreted: in fact, the use of glutaraldehyde for tissue preparation is thought to cause changes in docked vesicle measures due to its ability to cross-link proteins.

While the initial drop in PTP could be explained by impaired vesicle replenishment (Vasileva et al., 2012), we also observed a second, increased PTP phase (Fig. 3a,b). Alongside the RRP, also release probability and quantal size are increased during mossy fiber PTP (Vandael et al., 2020). Both could be elevated by default in SynTKO animals and increase PTP in the second phase. Interestingly, we detected an increase in active zone density and an increase in the RRP correlate upon FSK incubation in SynTKO boutons (Fig. 5g), which most likely reflects a change in the number of release sites. Hence, after overcoming the initial drop in PTP, other mechanisms could be untamed in SynTKO mossy fiber boutons, leading to enhanced PTP in a later phase.

The increased active zone density in SynTKO animals (Fig. 5e) could indicate a preset potentiated state (Orlando et al., 2021) due to homeostatic adaptation, similar to mechanisms in the calyx of Held of SynTKO animals (Vasileva et al., 2012). The active zone density was further increased when chemically potentiating SynTKO mossy fibers with FSK, leading to significantly higher densities than in FSK-treated WT boutons and untreated SynTKO boutons (Fig. 5e). An increase in the RRP correlate and active zone density after potentiation might also explain, to some extent, the increased LTP we observe in SynTKO animals (Figs. 3, 5e,g). Mossy fiber LTP has been analyzed previously in SynI KO (Takei et al., 1995) and SynDKO mice (Spillane et al., 1995) but was found to be unchanged. Thus, we speculate that the increase in LTP can only be detected upon the complete loss of synapsins.

Altogether our data suggest that, after overcoming the initial drop in PTP, other mechanisms could lead to enhanced PTP and LTP in SynTKO mossy fiber boutons.

It is unknown which mechanisms are shared between mossy fiber PTP and LTP. Synapsins might have specific functions in both processes, preventing excess release and balancing potentiation. Recent literature suggests that (1) diversity in STP depends on priming and fusion steps (Lin et al., 2022) and (2) increased fusion competence might underlie mossy fiber LTP, possibly mediated by Munc13-1 (Lipstein et al., 2021; Papantoniou et al., 2023; Fukaya et al., 2023a). Do synapsins—or specific synapsin isoforms—play a role in the regulation of vesicle docking, priming, and/or the insertion of new active zones at mossy fibers? Future work is needed to address these questions more specifically.

Here, we investigated plasticity at a glutamatergic synapse expressing SynIII in adulthood. We used SynTKO instead of SynIII KO animals to exclude compensatory effects via remaining synapsin isoforms. By combining physiological recordings—well-suited to record mossy fiber transmission (Breustedt et al., 2010)—and 3D ultrastructural analysis, our experiments shed light on synapsin-dependent plasticity from different angles. Our ultrastructural analysis is limited by the fact that chemical fixation is not the best method to investigate docked vesicles due to possible structural reorganization in the nanometer range, caused by glutaraldehyde-induced protein cross-linking. Another limitation is the limited volume of our partial 3D reconstruction. Future studies should utilize (1) high pressure freezing to draw more detailed conclusions regarding synapsins' role in the pool engram regulation and (2) volume electron microscopy data to assess morphological changes in 3D reconstructions of whole boutons.

To exclude possible indirect estrogen effects on mossy fiber plasticity (Harte-Hargrove et al., 2013), we used male mice only, limiting the generalizability. Future studies should include female animals. Finally, although the chemical induction of mossy fiber potentiation using FSK is widely used, it is still unclear if it shares the same mechanisms as electrically induced potentiation (Shahoha et al., 2022; Fukaya et al., 2023b). The scope of this study was limited to the characterization of SynTKO and does not directly compare the structure and function of mossy fiber boutons in SynIII and SynI and II DKO. Further work is needed to dissect the precise role of the various synapsin isoforms both in hippocampal mossy fiber boutons and in other synapses (Pieribone et al., 2002).

In summary, our work revealed that the complete loss of synapsins leads to disruption of presynaptic plasticity at hippocampal mossy fibers. Facilitation and PTP are reduced, but LTP is increased, in concert with an elevated active zone

density as well as an increased RRP correlate after FSK treatment. Our work contributes to a better understanding of mossy fiber presynaptic plasticity and, consequently, to a better understanding of synapsins' roles in learning and memory.

Data Availability

Data is fully available on request. Data tables and scripts for statistical analysis are available on GitHub: https://github.com/FeliBrue/Bruentgens_et_al_2024/.

References

- Aarts E, Verhage M, Veenvliet JV, Dolan CV, Van Der Sluis S (2014) A solution to dependency: using multilevel analysis to accommodate nested data. *Nat Neurosci* 17:491–496.
- Acsády L, Káli S (2007) Models, structure, function: the transformation of cortical signals in the dentate gyrus. *Prog Brain Res* 163:577–599.
- Acsády L, Kamondi A, Sik A, Freund T, Buzsáki G (1998) GABAergic cells are the major postsynaptic targets of mossy fibers in the rat hippocampus. *J Neurosci* 18:3386–3403.
- Amaral DG, Ishizuka N, Claiborne B (1990) Chapter neurons, numbers and the hippocampal network. *Prog Brain Res* 83:1–11.
- Atias M, Tevet Y, Sun J, Stavsky A, Tal S, Kahn J, Roy S, Gitler D (2019) Synapsins regulate α -synuclein functions. *Proc Natl Acad Sci U S A* 166:11116–11118.
- Baldelli P, Fassio A, Valtorta F, Benfenati F (2007) Lack of synapsin I reduces the readily releasable pool of synaptic vesicles at central inhibitory synapses. *J Neurosci* 27:13520–13531.
- Bates D, Mächler M, Bolker BM, Walker SC (2015) Fitting linear mixed-effects models using lme4. *J Stat Softw* 67:1–48.
- Benjamini Y, Hochberg Y (1995) Controlling the false discovery rate: a practical and powerful approach to multiple testing. *J R Stat Soc Ser B* 57:289–300.
- Boido D, Farisello P, Cesca F, Ferrea E, Valtorta F, Benfenati F, Baldelli P (2010) Cortico-hippocampal hyperexcitability in synapsin I/II/III knockout mice: age-dependency and response to the antiepileptic drug levetiracetam. *Neuroscience* 171:268–283.
- Breustedt J, Gundlfinger A, Varoqueaux F, Reim K, Brose N, Schmitz D (2010) Munc13-2 differentially affects hippocampal synaptic transmission and plasticity. *Cereb Cortex* 20:1109–1120.
- Browning MD, Huang CK, Greengard P (1987) Similarities between protein IIIa and protein IIIb, two prominent synaptic vesicle-associated phosphoproteins. *J Neurosci* 7:847–853.
- Bykhovskaia M (2011) Synapsin regulation of vesicle organization and functional pools. *Semin Cell Dev Biol* 22:387–392.
- Cesca F, Baldelli P, Valtorta F, Benfenati F (2010) The synapsins: key actors of synapse function and plasticity. *Prog Neurobiol* 91:313–348.
- Chamberland S, Evstratova A, Tóth K (2017) Short-term facilitation at a detonator synapse requires the distinct contribution of multiple types of voltage-gated calcium channels. *J Neurosci* 37:4913–4927.
- Cheng Q, Song S, Augustine GJ (2018) Molecular mechanisms of short-term plasticity: role of synapsin phosphorylation in augmentation and potentiation of spontaneous glutamate release. *Front Synaptic Neurosci* 10:33.
- Chi P, Greengard P, Ryan TA (2001) Synapsin dispersion and re-clustering during synaptic activity. *Nat Neurosci* 4:1187–1193.
- De Camilli P, Benfenati F, Valtorta F, Greengard P (1990) The synapsins. *Annu Rev Cell Biol* 6:433–460.
- De Camilli P, Cameron R, Greengard P (1983) Synapsin I (protein I), a nerve terminal-specific phosphoprotein. I. Its general distribution in synapses of the central and peripheral nervous system demonstrated by immunofluorescence in frozen and plastic sections. *J Cell Biol* 96:1337–1354.
- Dobrunz LE, Stevens CF (1997) Heterogeneity of release probability, facilitation, and depletion at central synapses. *Neuron* 18:995–1008.
- Farisello P, Boido D, Nieuws T, Medrihan L, Cesca F, Valtorta F, Baldelli P, Benfenati F (2013) Synaptic and extrasynaptic origin of the excitation/inhibition imbalance in the hippocampus of synapsin I/II/III knockout mice. *Cereb Cortex* 23:581–593.
- Fassio A, Raimondi A, Lignani G, Benfenati F, Baldelli P (2011) Synapsins: from synapse to network hyperexcitability and epilepsy. *Semin Cell Dev Biol* 22:408–415.
- Feng J, et al. (2002) Regulation of neurotransmitter release by synapsin III. *J Neurosci* 22:4372–4380.
- Ferreira A, Kao HT, Feng J, Rapoport M, Greengard P (2000) Synapsin III: developmental expression, subcellular localization, and role in axon formation. *J Neurosci* 20:3736–3744.
- Fukaya R, Hirai H, Sakamoto H, Hashimoto-dani Y, Hirose K, Sakaba T (2023a) Increased vesicle fusion competence underlies long-term potentiation at hippocampal mossy fiber synapses. *Sci Adv* 9:eadd3616.
- Fukaya R, Miyano R, Hirai H, Sakaba T (2023b) Mechanistic insights into cAMP-mediated presynaptic potentiation at hippocampal mossy fiber synapses. *Front Cell Neurosci* 17:1237589.
- Galbraith S, Daniel JA, Vissel B (2010) A study of clustered data and approaches to its analysis. *J Neurosci* 30:10601–10608.
- Gitler D, Takagishi Y, Feng J, Ren Y, Rodriguiz RM, Wetsel WC, Greengard P, Augustine GJ (2004) Different presynaptic roles of synapsins at excitatory and inhibitory synapses. *J Neurosci* 24:11368–11380.
- Glasgow SD, McPhedrain R, Madranges JF, Kennedy TE, Ruthazer ES (2019) Approaches and limitations in the investigation of synaptic transmission and plasticity. *Front Synaptic Neurosci* 11:20.
- Griffith WH (1990) Voltage-clamp analysis of posttetanic potentiation of the mossy fiber to CA3 synapse in hippocampus. *J Neurophysiol* 63:491–501.
- Hallermann S, Pawlu C, Jonas P, Heckmann M (2003) A large pool of releasable vesicles in a cortical glutamatergic synapse. *Proc Natl Acad Sci U S A* 100:8975–8980.
- Hanse E, Gustafsson B (2001) Paired-pulse plasticity at the single release site level: an experimental and computational study. *J Neurosci* 21:8362–8369.
- Harte-Hargrove LC, MacLusky NJ, Scharfman HE (2013) Brain-derived neurotrophic factor-estrogen interactions in the hippocampal mossy fiber pathway: implications for normal brain function and disease. *Neuroscience* 239:46–66.
- Heidari S, Babor TF, De Castro P, Tort S, Curno M (2016) Sex and gender equity in research: rationale for the SAGER guidelines and recommended use. *Res Integr Peer Rev* 1:2.
- Henze DA, Wittner L, Buzsáki G (2002) Single granule cells reliably discharge targets in the hippocampal CA3 network in vivo. *Nat Neurosci* 5:790–795.
- Hirokawa N, Sobue K, Kanda K, Harada A, Yorifuji H (1989) The cytoskeletal architecture of the presynaptic terminal and molecular structure of synapsin 1. *J Cell Biol* 108:111–126.
- Hosaka M, Hammer RE, Südhof TC (1999) A phospho-switch controls the dynamic association of synapsins with synaptic vesicles. *Neuron* 24:377–387.

- Imbrosci B, Schmitz D, Orlando M (2022) Automated detection and localization of synaptic vesicles in electron microscopy images. *eNeuro* 9:ENEURO.0400-20.2021.
- Jackman SL, Regehr WG (2017) The mechanisms and functions of synaptic facilitation. *Neuron* 94:447–464.
- Jung MW, McNaughton BL (1993) Spatial selectivity of unit activity in the hippocampal granular layer. *Hippocampus* 3:165–182.
- Kamiya H, Shinozaki H, Yamamoto C (1996) Activation of metabotropic glutamate receptor type 2/3 suppresses transmission at rat hippocampal mossy fiber synapses. *J Physiol* 493:447–455.
- Kao HT, Porton B, Czernik AJ, Feng J, Yiu G, Häring M, Benfenati F, Greengard P (1998) A third member of the synapsin gene family. *Proc Natl Acad Sci U S A* 95:4667–4672.
- Kielland A, Erisir A, Walaas SI, Heggelund P (2006) Synapsin utilization differs among functional classes of synapses on thalamocortical cells. *J Neurosci* 26:5786–5793.
- Kim O, Okamoto Y, Brose N, Shigemoto R, Jonas P (2023) Presynaptic cAMP-PKA-mediated potentiation induces reconfiguration of synaptic vesicle pools and channel-vesicle coupling at hippocampal mossy fiber boutons. *bioRxiv*.
- Krzywinski M, Altman N, Blainey P (2014) Points of significance: nested designs. *Nat Methods* 11:977–978.
- Lassalle JM, Bataille T, Halley H (2000) Reversible inactivation of the hippocampal mossy fiber synapses in mice impairs spatial learning, but neither consolidation nor memory retrieval, in the Morris navigation task. *Neurobiol Learn Mem* 73:243–257.
- Lazic SE (2010) The problem of pseudoreplication in neuroscientific studies: is it affecting your analysis? *BMC Neurosci* 11:5.
- Li L, et al. (1995) Impairment of synaptic vesicle clustering and of synaptic transmission, and increased seizure propensity, in synapsin I-deficient mice. *Proc Natl Acad Sci U S A* 92:9235–9239.
- Lin KH, Taschenberger H, Neher E (2022) A sequential two-step priming scheme reproduces diversity in synaptic strength and short-term plasticity. *Proc Natl Acad Sci U S A* 119:e2207987119.
- Lipstein N, Chang S, Lin K-H, López-Murcia FJ, Neher E, Taschenberger H, Brose N (2021) Munc13-1 is a Ca²⁺-phospholipid-dependent vesicle priming hub that shapes synaptic short-term plasticity and enables sustained neurotransmission. *Neuron* 109:3980–4000.e7.
- Longfield SF, et al. (2024) Synapsin 2a tetramerisation selectively controls the presynaptic nanoscale organisation of reserve synaptic vesicles. *Nat Commun* 15:2217.
- Matos H, Quiles R, Andrade R, Bykhovskaia M (2019) Growth and excitability at synapsin II deficient hippocampal neurons. *Mol Cell Neurosci* 96:25–34.
- Medrihan L, Cesca F, Raimondi A, Lignani G, Baldelli P, Benfenati F (2013) Synapsin II desynchronizes neurotransmitter release at inhibitory synapses by interacting with presynaptic calcium channels. *Nat Commun* 4:1512.
- Medrihan L, Ferrea E, Greco B, Baldelli P, Benfenati F (2015) Asynchronous GABA release is a key determinant of tonic inhibition and controls neuronal excitability: a study in the synapsin II^{-/-} mouse. *Cereb Cortex* 25:3356–3368.
- Milovanovic D, Wu Y, Bian X, De Camilli P (2018) A liquid phase of synapsin and lipid vesicles. *Science* 361:604–607.
- Monday HR, Kharod SC, Yoon YJ, Singer RH, Castillo PE (2022) Presynaptic FMRP and local protein synthesis support structural and functional plasticity of glutamatergic axon terminals. *Neuron* 110:2588–2606.e6.
- Monday HR, Younts TJ, Castillo PE (2018) Long-term plasticity of neurotransmitter release: emerging mechanisms and contributions to brain function and disease. *Annu Rev Neurosci* 41:299–322.
- Mori M, Abegg MH, Gähwiler BH, Gerber U (2004) A frequency-dependent switch from inhibition to excitation in a hippocampal unitary circuit. *Nature* 431:453–456.
- Nadler JV (2003) The recurrent mossy fiber pathway of the epileptic brain. *Neurochem Res* 28:1649–1658.
- Neher E, Brose N (2018) Dynamically primed synaptic vesicle states: key to understand synaptic short-term plasticity. *Neuron* 100:1283–1291.
- Neher E, Sakaba T (2008) Multiple roles of calcium ions in the regulation of neurotransmitter release. *Neuron* 59:861–872.
- Nicoll RA, Schmitz D (2005) Synaptic plasticity at hippocampal mossy fibre synapses. *Nat Rev Neurosci* 6:863–876.
- Nikolaev M, Heggelund P (2015) Functions of synapsins in corticothalamic facilitation: important roles of synapsin I. *J Physiol* 593:4499–4510.
- Orlando M, Dvorzhak A, Bruentgens F, Maglione M, Rost BR, Sigrist SJ, Breustedt J, Schmitz D (2021) Recruitment of release sites underlies chemical presynaptic potentiation at hippocampal mossy fiber boutons. *PLoS Biol* 19:e3001149.
- Owe SG, Jensen V, Evergren E, Ruiz A, Shupliakov O, Kullmann DM, Storm-Mathisen J, Walaas SI, Hvalby O, Bergersen LH (2009) Synapsin- and actin-dependent frequency enhancement in mouse hippocampal mossy fiber synapses. *Cereb Cortex* 19:511–523.
- Papantoniou C, et al. (2023) Munc13- and SNAP25-dependent molecular bridges play a key role in synaptic vesicle priming. *Sci Adv* 9:eadf6222.
- Pechstein A, Tomilin N, Fredrich K, Vorontsova O, Sopova E, Evergren E, Haucke V, Brodin L, Shupliakov O (2020) Vesicle clustering in a living synapse depends on a synapsin region that mediates phase separation. *Cell Rep* 30:2594–2602.e3.
- Percie du Sert N, et al. (2020) The arrive guidelines 2.0: updated guidelines for reporting animal research. *PLoS Biol* 18:e3000410.
- Piccini A, Perlini LE, Cancedda L, Benfenati F, Giovedi S (2015) Phosphorylation by PKA and Cdk5 mediates the early effects of synapsin III in neuronal morphological maturation. *J Neurosci* 35:13148–13159.
- Pieribone VA, Porton B, Rendon B, Feng J, Greengard P, Kao HT (2002) Expression of synapsin III in nerve terminals and neurogenic regions of the adult brain. *J Comp Neurol* 454:105–114.
- Pieribone VA, Shupliakov O, Brodin L, Hilfiker-Rothenfluh S, Czernik AJ, Greengard P (1995) Distinct pools of synaptic vesicles in neurotransmitter release. *Nature* 375:493–497.
- Rollenhagen A, Sätzler K, Rodríguez EP, Jonas P, Frotscher M, Lübke JHR (2007) Structural determinants of transmission at large hippocampal mossy fiber synapses. *J Neurosci* 27:10434–10444.
- Rolls ET (2018) The storage and recall of memories in the hippocampocortical system. *Cell Tissue Res* 373:577–604.
- Rosahl TW, Geppert M, Spillane D, Herz J, Hammer RE, Malenka RC, Südhof TC (1993) Short-term synaptic plasticity is altered in mice lacking synapsin I. *Cell* 75:661–670.
- Rosahl TW, Spillane D, Missler M, Herz J, Selig DK, Wolff JR, Hammer RE, Malenka RC, Südhof TC (1995) Essential functions of synapsins I and II in synaptic vesicle regulation. *Nature* 375:488–493.
- Salin PA, Scanziani M, Malenka RC, Nicoll RA (1996) Distinct short-term plasticity at two excitatory synapses in the hippocampus. *Proc Natl Acad Sci U S A* 93:13304–13309.
- Sansevino R, Hoffmann C, Milovanovic D (2023) Condensate biology of synaptic vesicle clusters. *Trends Neurosci* 46:293–306.
- Shahoha M, Cohen R, Ben-Simon Y, Ashery U (2022) cAMP-dependent synaptic plasticity at the hippocampal mossy fiber terminal. *Front Synaptic Neurosci* 14:861215.
- Sihra TS, Wang JKT, Gorelick FS, Greengard P (1989) Translocation of synapsin I in response to depolarization of isolated nerve terminals. *Proc Natl Acad Sci U S A* 86:8108–8112.
- Siksou L, et al. (2007) Three-dimensional architecture of presynaptic terminal cytomatrix. *J Neurosci* 27:6868–6877.
- Song SH, Augustine GJ (2015) Synapsin isoforms and synaptic vesicle trafficking. *Mol Cells* 38:936–940.
- Song SH, Augustine GJ (2023) Different mechanisms of synapsin-induced vesicle clustering at inhibitory and excitatory synapses. *Cell Rep* 42:113004.
- Spillane DM, Rosahl TW, Südhof TC, Malenka RC (1995) Long-term potentiation in mice lacking synapsins. *Neuropharmacology* 34:1573–1579.

- Südhof TC, et al. (1989) Synapsins: mosaics of shared and individual domains in a family of synaptic vesicle phosphoproteins. *Science* 245:1474–1480.
- Sun J, Bronk P, Liu X, Han W, Südhof TC (2006) Synapsins regulate use-dependent synaptic plasticity in the calyx of Held by a Ca²⁺/calmodulin-dependent pathway. *Proc Natl Acad Sci U S A* 103:2880–2885.
- Sun HY, Lyons SA, Dobrunz LE (2005) Mechanisms of target-cell specific short-term plasticity at Schaffer collateral synapses onto interneurons versus pyramidal cells in juvenile rats. *J Physiol* 568:815–840.
- Takei Y, Harada A, Takeda S, Kobayashi K, Terada S, Noda T, Takahashi T, Hirokawa N (1995) Synapsin I deficiency results in the structural change in the presynaptic terminals in the murine nervous system. *J Cell Biol* 131:1789–1800.
- Terada S, Tsujimoto T, Takei Y, Takahashi T, Hirokawa N (1999) Impairment of inhibitory synaptic transmission in mice lacking synapsin I. *J Cell Biol* 145:1039–1048.
- Torborg CL, Nakashiba T, Tonegawa S, McBain CJ (2010) Control of CA3 output by feedforward inhibition despite developmental changes in the excitation–inhibition balance. *J Neurosci* 30:15628–15637.
- Toth K, Soares G, Lawrence JJ, Philips-Tansey E, McBain CJ (2000) Differential mechanisms of transmission at three types of mossy fiber synapse. *J Neurosci* 20:8279–8289.
- Valente P, Casagrande S, Nieuwenhuis T, Verstegen AMJ, Valtorta F, Benfenati F, Baldelli P (2012) Site-specific synapsin I phosphorylation participates in the expression of post-tetanic potentiation and its enhancement by BDNF. *J Neurosci* 32:5868–5879.
- Vandaele D, Borges-Merjane C, Zhang X, Jonas P (2020) Short-term plasticity at hippocampal mossy fiber synapses is induced by natural activity patterns and associated with vesicle pool engram formation. *Neuron* 107:509–521.e7.
- Vasileva M, Horstmann H, Geumann C, Gitler D, Kuner T (2012) Synapsin-dependent reserve pool of synaptic vesicles supports replenishment of the readily releasable pool under intense synaptic transmission. *Eur J Neurosci* 36:3005–3020.
- Vyleta NP, Borges-Merjane C, Jonas P (2016) Plasticity-dependent, full detonation at hippocampal mossy fiber-CA3 pyramidal neuron synapses. *Elife* 5:e17977.
- Weisskopf MG, Castillo PE, Zalutsky RA, Nicoll RA (1994) Mediation of hippocampal mossy fiber long-term potentiation by cyclic AMP. *Science* 265:1878–1882.
- Wesseling JF, Lo DC (2002) Limit on the role of activity in controlling the release-ready supply of synaptic vesicles. *J Neurosci* 22:9708–9720.
- Zalutsky RA, Nicoll RA (1990) Comparison of two forms of long-term potentiation in single hippocampal neurons. *Science* 248:1619–1624.
- Zhang M, Augustine GJ (2021) Synapsins and the synaptic vesicle reserve pool: floats or anchors? *Cells* 10:658.
- Zucker RS, Regehr WG (2002) Short-term synaptic plasticity. *Annu Rev Physiol* 64:355–405.